ISSN 1674-1056
http://cpb.iphy.ac.cn
http://iopscience.iop.org/cpb
中国物理 B
Chinese Physics
中国物理 Chinese Physics B

Quantum computation and simulation with superconducting qubits

Kaiyong He(何楷泳), Xiao Geng(耿霄), Rutian Huang(黄汝田), Jianshe Liu(刘建设), and Wei Chen(陈炜)
Citation: Chin. Phys. B, 2021, 30 (**8**): 080304. DOI: 10.1088/1674-1056/ac16cf
Journal homepage: http://cpb.iphy.ac.cn; http://iopscience.iop.org/cpb

What follows is a list of articles you may be interested in

Optimized pulse for stimulated Raman adiabatic passage on noisy experimental platform

Zhi-Ling Wang(王志凌), Leiyinan Liu(刘雷轶男), and Jian Cui(崔健)
Chin. Phys. B, 2021, 30 (**8**): 080305. DOI: 10.1088/1674-1056/abfccb

Universal quantum circuit evaluation on encrypted data using probabilistic quantum homomorphic encryption scheme

Jing-Wen Zhang(张静文), Xiu-Bo Chen(陈秀波), Gang Xu(徐刚), and Yi-Xian Yang(杨义先)
Chin. Phys. B, 2021, 30 (**7**): 070309. DOI: 10.1088/1674-1056/ac003b

Quantum computation and error correction based on continuous variable cluster states

Shuhong Hao(郝树宏), Xiaowei Deng(邓晓玮), Yang Liu(刘阳), Xiaolong Su(苏晓龙), Changde Xie(谢常德), and Kunchi Peng(彭堃墀)
Chin. Phys. B, 2021, 30 (**6**): 060312. DOI: 10.1088/1674-1056/abeb0a

Quantum computation and simulation with vibrational modes of trapped ions

Wentao Chen(陈文涛), Jaren Gan, Jing-Ning Zhang(张静宁), Dzmitry Matuskevich, and Kihwan Kim(金奇奂)
Chin. Phys. B, 2021, 30 (**6**): 060311. DOI: 10.1088/1674-1056/ac01e3

Efficient self-testing system for quantum computations based on permutations

Shuquan Ma(马树泉), Changhua Zhu(朱畅华), Min Nie(聂敏), and Dongxiao Quan(权东晓)
Chin. Phys. B, 2021, 30 (**4**): 040305. DOI: 10.1088/1674-1056/abe29a

---

TOPICAL REVIEW — Quantum computation and quantum simulation

Quantum computation and simulation with superconducting qubits*

Kaiyong He(何楷泳)[1,2,3,†], Xiao Geng(耿霄)[1,2,3,†], Rutian Huang(黄汝田)[1,2,3], Jianshe Liu(刘建设)[1,2,3], and Wei Chen(陈炜)[1,2,3,‡]

[1] School of Integrated Circuits, Tsinghua University, Beijing 100084, China
[2] Beijing National Research Center for Information Science and Technology, Beijing 100084, China
[3] Tsinghua University Future Chip Technology Advanced Innovation Center, Beijing 100084, China

(Received 20 April 2021; revised manuscript received 13 July 2021; accepted manuscript online 22 July 2021)

Superconducting circuits based on Josephson junctions are regarded as one of the most promising technologies for the implementation of scalable quantum computers. This review presents the basic principles of superconducting qubits and shows the progress of quantum computing and quantum simulation based on superconducting qubits in recent years. The experimental realization of gate operations, readout, error correction codes, as well as some quantum algorithms are summarized, followed by an introduction of quantum simulation. And then some important applications in fields including condensed matter physics, quantum annealing, and quantum chemistry are discussed.

Keywords: quantum computation, quantum simulation, superconducting qubit

PACS: 03.67.Lx, 03.67.Ac, 85.25.−j, 85.25.Cp **DOI:** 10.1088/1674-1056/ac16cf

1. Introduction

In recent years, superconducting quantum computation and simulation have developed rapidly, which have entered the noisy intermediate-scale quantum (NISQ) era.[1] In the NISQ era, 50–100 qubits without error correction can perform some tasks that demonstrate the superior ability of quantum computers. Quantum supremacy has shown that in some tasks, quantum computer could surpass the most powerful classical computers.[2] Another most anticipated application in the NISQ era is quantum simulation, such as exploring many-body quantum physics, quantum chemistry, and so on.[3] However, quantum devices still suffer from noise, and the sizes of the circuits are limited.

In this paper, we focus on some important heuristic advances in the field. In Section 2, basic concepts of superconducting qubits as well as their operation and readout are introduced. In Section 3, experimental realization without error correction of some quantum algorithms, including Deutsch–Jozsa (D-J) algorithm, Grover algorithm, Shor algorithm, and Harrow–Hassidim–Lloyd (HHL) algorithm are summarized. A brief introduction of quantum error correction methods including the Calderbank–Shor–Steane codes (CSS) codes, the surface codes, and Bosonic quantum codes are discussed, followed by a review of two different kinds of quantum simulations, digital and analog quantum simulations, in Section 4.

2. Superconducting qubit

2.1. Three basic types of superconducting qubits

There are three types of basic superconducting qubits, i.e., the charge qubit, the flux qubit, and the phase qubit, classified according to the "controlled variable", i.e., the qubit variable for manipulating quantum information.[4] The key element in a superconducting qubit is the Josephson junction, which is a non-dissipative and strongly non-linear superconducting device. Its behavior can be described by the Josephson equation

$$I = I_{\mathrm{c}} \sin\left[\frac{2\pi}{\Phi_0}\int_{-\infty}^{t} V\left(t'\right)\mathrm{d}t'\right], \tag{1}$$

where I_{c} is the critical current of the Josephson junction and $\Phi_0 = h/2e$ is the flux quantum. In general, the Hamiltonian of a circuit could be represented with "node voltage" V and the conjugate "node current" I. However, for a circuit with Josephson junction, a representation based on "node flux" Φ and "node charge" Q would be much more convenient,[5,6] where

$$\Phi = \int_{-\infty}^{t} V\left(t'\right)\mathrm{d}t', \tag{2a}$$

$$Q = \int_{-\infty}^{t} I\left(t'\right)\mathrm{d}t'. \tag{2b}$$

To get a quantum-mechanical description of a circuit, one can use the quantum operators $\Phi \to \hat{\Phi}$ and $Q \to \hat{Q}$, which obey the commutation relation $\left[\hat{\Phi}, \hat{Q}\right] = \mathrm{i}\hbar$. $\hat{\Phi}$ plays the role

*Project supported by the National Natural Science Foundation of China (Grant Nos. 11653001, 11653004, and 60836001).
†These authors contributed equally.
‡Corresponding author. E-mail: weichen@mail.tsinghua.edu.cn
© 2021 Chinese Physical Society and IOP Publishing Ltd

of general position while $\hat{Q}$ plays the role of conjugate momentum. For some special cases, the dimensionless electric variables $\hat{\phi} \equiv 2\pi\hat{\Phi}/\Phi_0$ and $\hat{n} \equiv \hat{Q}/2e$ would be more useful, and thus, the commutation relation turns to $[\hat{\phi}, \hat{n}] = \mathrm{i}$.

2.1.1. Charge qubit

The basic schematic of a charge qubit, also named as Cooper-pair box,[7,8] is shown in Fig. 1, where a Josephson junction is connected to a small superconducting island and a large superconducting reservoir, while the voltage source controls the charge offset $n_\mathrm{g} = C_\mathrm{g}V_\mathrm{g}/2e$ on the island capacitively.[8]

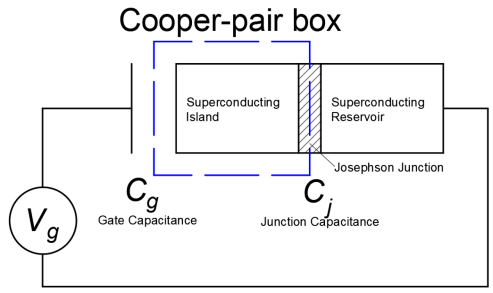


Fig. 1. Schematic of the single Cooper-pair box.

The Hamiltonian of the system is

$$\hat{H} = 4E_\mathrm{C}\left(\hat{n} - n_\mathrm{g}\right)^2 - E_\mathrm{J}\cos\hat{\phi}, \tag{3}$$

where $\hat{n}$ is the excess number of Cooper pairs on the island, $\hat{\phi} \equiv 2\pi\hat{\Phi}/\Phi_0$ is the gauge-invariant phase across the junction, $E_\mathrm{J} = I_\mathrm{c}\Phi_0/2\pi$ is the Josephson energy, and $E_\mathrm{C} = e^2/2C_\Sigma$ is the charging energy per electron required to add a Cooper pair to the superconducting island. $C_\Sigma = C_\mathrm{g} + C_\mathrm{j}$ is the total island capacitance, where C_g is the gate capacitance and C_j is the junction capacitance, as shown in Fig. 1. For a charge qubit, the typical ratio of Josephson energy to charging energy $E_\mathrm{J}/E_\mathrm{C}$ is about 1, and thus the charging energy dominates. The corresponding ratio of eigenenergy E_m to transition energy E_{01} ($E_1 - E_0$ at $n_\mathrm{g} = 0.5$) of the qubit is plotted in Fig. 2(a). Other ratios E_m/E_{01} for different $E_\mathrm{J}/E_\mathrm{C}$ (5, 10, and 50) are also plotted in Figs. 2(b)–2(d). Since $\hat{\phi}$ and $\hat{n}$ satisfy the commutation relation $[\hat{\phi}, \hat{n}] = \mathrm{i}$, the charge number is a good quantum number and the fluctuation of the phase is relatively large. The Josephson junction is often substituted by a dc-SQUID (superconducting quantum interference device) which can be regarded as a tunable Josephson junction, increasing the flexibility of manipulating the charge qubit.

In the so-called charge basis,[4] $\hat{n} = \Sigma_n n|n\rangle\langle n|$, and $\cos\hat{\phi} = 1/2 \cdot \Sigma_n(|n\rangle\langle n+1| + |n+1\rangle\langle n|)$, the Hamiltonian can be written as

$$\hat{H} = \Sigma_n\Big[4E_\mathrm{C}\left(n - n_\mathrm{g}\right)^2|n\rangle\langle n| - \frac{1}{2}E_\mathrm{J}(|n\rangle\langle n+1| + |n+1\rangle\langle n|)\Big]. \tag{4}$$

The charge qubit is typically biased at the "sweet spot" $n_\mathrm{g} \approx 1/2$. At the spot, for states $|n\rangle$ and $|n+1\rangle$, the first term of the Hamiltonian is degenerate while the degeneracy is broken by the second term. The two lowest-energy levels are far separated from the others when $E_\mathrm{J} \ll E_\mathrm{C}$ such that they could form a qubit. In addition, the transition frequency of the system is insensitive to the offset-charge noise to the first order at the sweet spot, leading to a longer coherence time. However, $E_\mathrm{J}/E_\mathrm{C}$ cannot be too small, or the high order of offset-charge noise will be significant.

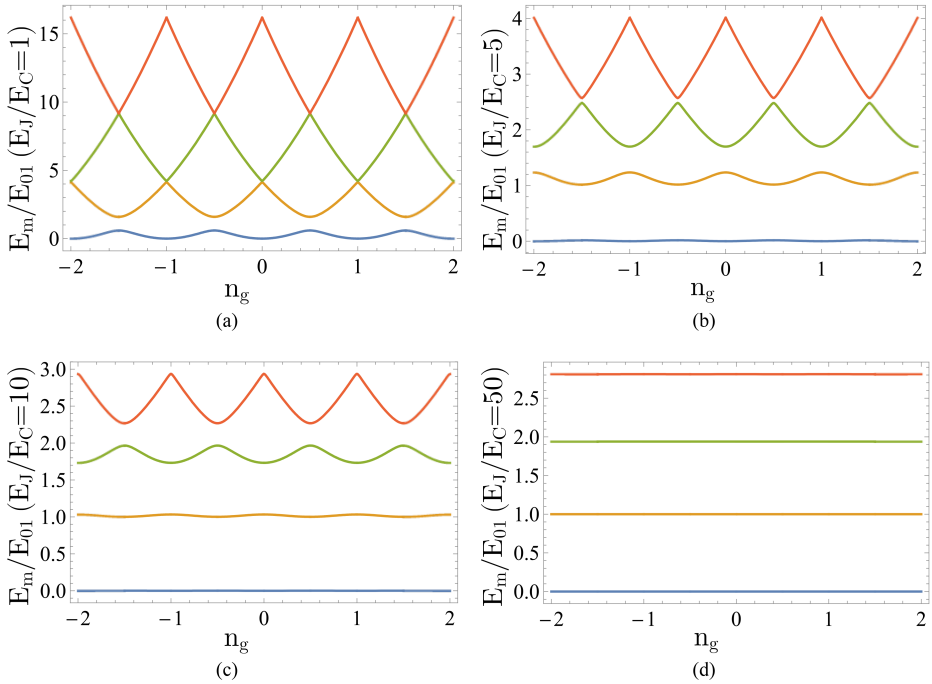


Fig. 2. Eigenenergies of Cooper-pair boxes changed by charge offset n_g on the gate for different ratios $E_\mathrm{J}/E_\mathrm{C}$.

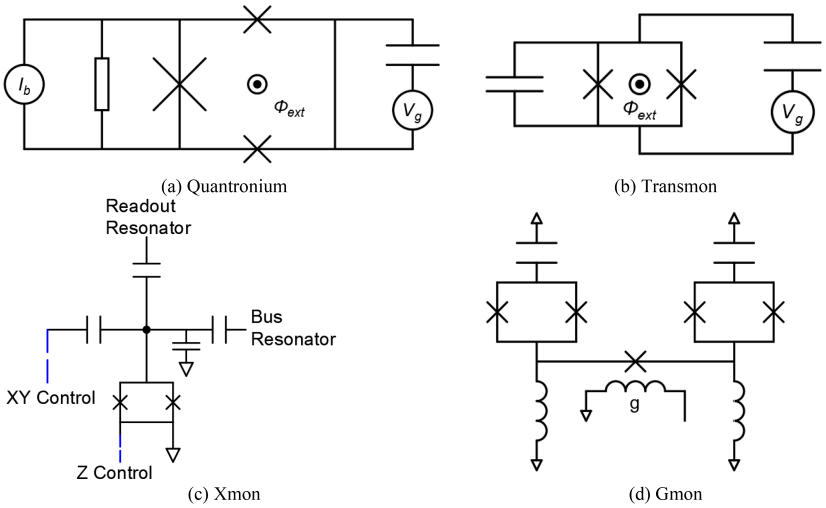


Fig. 3. Improved qubits based on charge qubits.

There are some improved qubits based on charge qubit for longer coherence time, easy connectivity, fast control, and high-fidelity readout. The first significantly improved qubit is the "quantronium"[9,10] which is shown in Fig. 3(a). It is a three-junction circuit in which two small junctions define the Cooper pair box coupled to the write and control port and a large junction is coupled to the readout port. The coherence time is improved by two orders of magnitude to hundreds of nanoseconds compared to the basic charge qubit whose coherence time is about 1 ns.

Another important improvement of charge qubit is called "transmon"[11] (transmission-line shunted plasma oscillation qubit). A large capacitor is shunted to the charge qubit to increase the ratio $E_{\rm J}/E_{\rm C}$ properly, as shown in Fig. 3(b). Since the sensitivity to the offset-charge noise reduces exponentially with the increase of $E_{\rm J}/E_{\rm C}$, while the anharmonicity only deteriorates by a weak power law, the advantage dominates. The coherence time of the qubit is increased to tens of μs. The transmon is embedded in a transmission line, which makes control and readout very convenient. A new qubit design based on transmon is Xmon,[12] shown in Fig. 3(c) that has a cross shape structure. Two of the arms are for XY control and Z control. The arm coupling to a resonator is for readout and the last arm can couple to other qubits. In such a schematic, the operations, readout and coupling are all convenient and efficient. A Josephson junction can be added between two Xmons to get fast tunable coupling, high coherence, and minimal cross talk, as shown in Fig. 3(d), which is called Gmon.[13,14] In recent years, qubits based on charge-qubit have developed rapidly, showing their potential in quantum computation.

2.1.2. Flux qubit

A flux qubit consists of a superconducting loop interrupted by one or more Josephson junctions, as shown in Fig. 4(a).[15–17] It can be considered as the dual of the charge qubit, and the Hamiltonian of the circuit can be written as

$$\hat{H} = \frac{\hat{Q}^2}{2C_{\rm J}} + \frac{\hat{\Phi}^2}{2L} - E_{\rm J}\cos\left[\frac{2e}{\hbar}\left(\hat{\Phi} - \Phi_{\rm ext}\right)\right], \tag{5}$$

where $\Phi_{\rm ext}$ represents the external applied flux through the superconducting loop. From the Hamiltonian, one can see that the potential of the flux qubit is composed of a parabolic potential and a cosine corrugation. The typical $E_{\rm J}/E_{\rm C}$ value of a flux qubit is about 50, and thus $\hat{\Phi}$ is a good quantum number and charge has large fluctuation. However, in different kinds of flux qubits, the $E_{\rm J}/E_{\rm C}$ value can vary considerably (from tens to thousands), and the main feature of a flux qubit is that its controlled variable is the flux.[15–22]

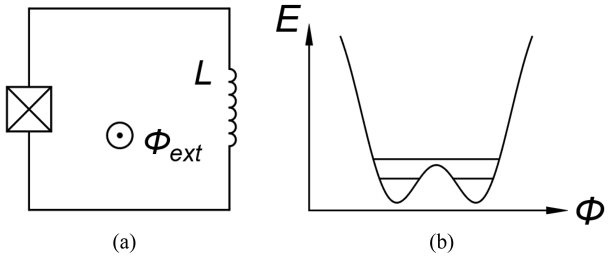


Fig. 4. Flux qubit.

The general feature of the potential of a simple flux qubit is shown in Fig. 4(b). When $\Phi_{\rm ext}/\Phi_0 \approx 0.5$ and in the two-level approximation, the qubit Hamiltonian is given by

$$\hat{H} = \varepsilon\left(\Phi_z\right)\sigma_z + \Delta\sigma_x, \tag{6}$$

where ε is the energy difference between the bottoms of two wells, a function of flux through the superconducting loop (denoted as Φ_z), and Δ is the tunneling-coupling strength between the two current states. Replacing the Josephson junction with a dc-SQUID loop, the qubit Hamiltonian becomes

$$\hat{H} = \varepsilon\left(\Phi_z, \Phi_x\right)\sigma_z + \Delta\left(\Phi_x\right)\sigma_x, \tag{7}$$

where Φ_x is the externally applied flux through the SQUID loop, as shown in Fig. 5. ε is not only a function of Φ_z, but

also of Φ_x, and Δ becomes *in situ* tunable now. Thus, the flux qubit is a spin-1/2 system with tunable z and x fields, which is also a proper building block for quantum annealing applications based on the transverse Ising Hamiltonian.

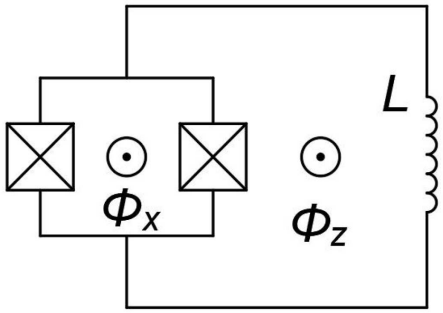
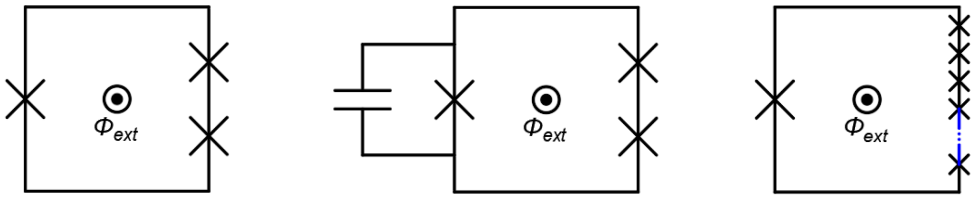


Fig. 5. Flux qubit whose Josephson junction is replaced by a dc-SQUID.

In general, a flux qubit needs a large self-inductance, which can be achieved with a large loop size to satisfy the flux quantization condition. However, a large loop will introduce more flux noise to the flux qubit, limiting the coherence time. A better choice is to put 3 junctions in the loop,[16,17] as shown in Fig. 6(a), in which the loop size is reduced and the flux quantization condition is satisfied by introducing two large Josephson junctions in the superconducting loop.

To reduce the sensitivity to charge noise and improve the device-to-device reproducibility, a large capacitor could be shunted to the smaller junction in the 3-junction flux qubit, resulting in a "capacitively shunted flux qubit", whose coherence time is in the range of 50 μs to 100 μs.[18–20] The schematic of such a C-shunt flux qubit is shown in Fig. 6(b). Another efficient way to reduce the influence of offset-charge noise is to shunt the small junction with a series array of large-capacitance tunnel junctions, resulting in a fluxonium,[21,22] as shown in Fig. 6(c).



(a) Three-junction Flux Qubit (b) C-shunt Flux Qubit (c) Fluxonium

Fig. 6. Improved qubits based on flux qubits.

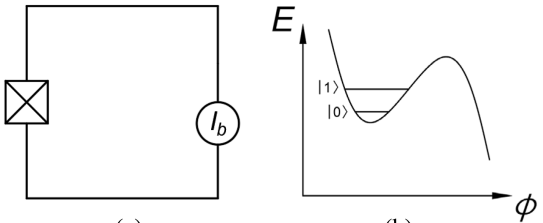
2.1.3. Phase qubit

The third basic type of superconducting qubits is the phase qubit,[23–27] which consists of a dc-current-biased Josephson junction, as shown in Fig. 7. Its coherent oscillation was observed in 2002.[23,24] The controlled variable of a phase qubit is the gauge-invariant phase $\hat{\phi} = 2\pi\hat{\Phi}/\Phi_0$. Since the ratio E_J/E_C is about 10^6, the good quantum number is the phase $\hat{\phi}$, and is insensitive to the offset-charge noise. The Hamiltonian of the circuit is

$$\hat{H} = \frac{\hat{Q}^2}{2C_J} - \frac{\Phi_0}{2\pi} I_b \hat{\phi} - E_J \cos\hat{\phi}. \tag{8}$$

The potential energy of the phase shows a "tilted washboard" shape, as shown in Fig. 7(b). It could be controlled by an applied dc-bias current I_b, which is usually set to be very close to the critical current $I_c = 2eE_J/\hbar$ to obtain a large non-linearity in the Josephson inductance. Neglecting the effect from higher levels, the two lowest levels in the potential well form a phase qubit. For $I_{bias} \approx I_c$, the barrier height is $\Delta U = \left(2\sqrt{2}/3\pi\right) I_c \Phi_0 \left(1 - I/I_c\right)^{3/2}$ and $\omega_p = \left(2\pi I_c/C\Phi_0\right)^{1/2} \left[1 - I/I_c\right]^{1/4}$.[23,27] In typical cases, the number of states in the well is $\Delta U/\hbar\omega_p \approx 3$.

There is a built-in readout in the phase qubit. When sending a probe signal to induce a transition to the higher level from $|1\rangle$ state, the tunneling probability through the potential well will increase rapidly. After tunneling, the phase runs down the washboard, leading to a voltage $V \neq 0$ appearing across the junction, which implies that the qubit was in state $|1\rangle$. If the qubit was in state $|0\rangle$, the voltage keeps zero.



(a) (b)

Fig. 7. Phase qubit.

When biasing the qubit with current, the qubit will dissipate strongly from the bias lead. An improved method is to bias the qubit with a magnetic flux.[23,28] It transforms the impedance, and thus provides isolation of the phase qubit from the environment. There is also a significant modification in the readout of phase qubit.[29,30] If the phase qubit is readout from voltage, quasiparticles are generated when the junction switched into the voltage states. They are found to influence the decoherence of the qubit. A better design is to readout with a SQUID separated from the qubit. The change of the circulating current in the qubit loop, which is generated from the

tunneling event, can be probed with the SQUID. The quasiparticles generated during the readout are kept away from the qubit, and thus increasing the decoherence time.

2.1.4. Other kinds of superconducting qubits

There are some other kinds of superconducting qubits. 0-π qubit is a qubit whose logical states are disjoint support so that it is exponentially protected from charge (flux) noise.[31,32] Quasicharge qubit exhibits the characteristics of the artificial atom which is dual with transmon.[33] The exploration of new kinds of qubits is still in progress, and the family of superconducting qubits is being broadened. With decades of development, the performance of superconducting qubits has increased gradually. Table 1 shows the decoherence time of superconducting qubits reported in recent years.

Table 1. Decoherence time of superconducting qubits.

Qubit	T_1 (μs)	T_2 (μs)	Group	Year
Transmon	55	60	IBM[34]	2013
Transmon	56.1	44.7	IBM[35]	2016
3D transmon	70	92	IBM[36]	2012
3D transmon	8100*		Yale[37]	2014
3D transmon	80	154	MIT[38]	2015
3D transmon	162		IBM[39]	2016
3D transmon	95	85	Yale[40]	2020
Xmon	44	20	UCSB[41]	2013
Xmon	49.4		UCSB[42]	2017
Flux qubit (C-shunt)	40	85	MIT[43]	2016
Fluxonium	500*	510*	Maryland[21]	2019
0-π	1560	25	Princeton[32]	2019
Quasicharge qubit	10	20	Maryland[33]	2020

The T_2 were obtained by spin echo measurements. The data with symbol * here are the best data in the corresponding literatures.

2.2. Gate operations

The gate operations and readout of superconducting qubits are implemented by applying microwave pulses, which could be described by circuit quantum electrodynamics (circuit-QED).[44,45] Usually, the qubit is coupled to a resonator and with microwave pulse applied to the resonator, one can realize gate operations and readout of the qubit. Under rotating wave approximation (RWA), the Hamiltonian of the coupled system is

$$\hat{H} = \frac{1}{2}\hbar\omega_{\mathrm{q}}\sigma_z + \hbar\omega_{\mathrm{r}}a^{+}a + \hbar g\left(a^{+}\sigma_{-} + a\sigma_{+}\right). \tag{9}$$

The first term is the Hamiltonian of the qubit, the second term represents the first mode of the resonator, neglecting the constant term, and the last term is the coupling Hamiltonian. g is the coupling strength between the qubit and the resonator. In a charge qubit frame, $g = g_{0,1} = eV_0/\hbar\cdot\beta$, where $V_0 = \sqrt{\hbar\omega_{\mathrm{r}}/cL}$ is the rms voltage of the microwave and $\beta = C_{\mathrm{g}}/(C_{\mathrm{J}}+C_{\mathrm{g}}+C_{\mathrm{B}})$.[46] In V_0, c is the capacitance per unit of the transmission line, and L is the length of the resonator. Thus, the coupling strength is dependent on the microwave voltage and coupling capacitance, which may vary in other situations. According to the last term, we could see that when the qubit is populated to the excited state, a photon is annihilated in the resonator, and while the qubit drops back to the ground state, a photon is created in the resonator. In this process, energy is conserved. In the following section, based on the Xmon qubits, we will discuss how to perform gate operation and readout on the qubits.

2.2.1. Single qubit operations

For Xmon, rotation in the XY direction is achieved by applying microwave via the waveguide on the left, as shown in Fig. 3(c).[47] Assuming that the microwave is[44]

$$\Omega(t) = \Omega_0\cos(\omega t+\gamma), \quad 0<t<t_0, \tag{10}$$

the Hamiltonian is

$$\hat{H}_{\mathrm{drive}} = \frac{1}{2}\hbar\omega_{\mathrm{q}}\sigma_z + \hbar\Omega_{\mathrm{Rabi}}\cos(\omega_{\mathrm{d}}t+\gamma)\sigma_x. \tag{11}$$

Turning to the rotation frame of the microwave and under rotating wave approximation, there is

$$\hat{H}_{\mathrm{drive}} = \frac{1}{2}\hbar\Delta_{\mathrm{q}}\sigma_z + \frac{1}{2}\hbar\Omega_{\mathrm{Rabi}}\left[\cos(\gamma)\sigma_x + \sin(\gamma)\sigma_y\right], \tag{12}$$

where $\Delta_{\mathrm{q}} = \omega_{\mathrm{q}} - \omega_{\mathrm{d}}$. Ω_{Rabi} is the Rabi frequency experienced by the qubit. Under this Hamiltonian, the unitary operator of the system is

$$\begin{aligned}\hat{U} &= \exp\left(-\frac{\mathrm{i}}{\hbar}\int_0^{t_0}\hat{H}_{\mathrm{drive}}(t')\,\mathrm{d}t'\right)\\ &= \exp\Big[-\frac{\mathrm{i}}{2}\left(\Delta_{\mathrm{q}}t_0\sigma_z + \Omega_{\mathrm{Rabi}}t_0\cos(\gamma)\sigma_x\right.\\ &\quad\left.+\Omega_{\mathrm{Rabi}}t_0\sin(\gamma)\sigma_y\right)\Big].\end{aligned} \tag{13}$$

When microwave and qubit are in resonance, i.e., $\Delta_{\mathrm{q}} = 0$ and tune the phase of microwave γ to be 0, it turns to a rotation operation along x axis, $\hat{U} = \exp(-\frac{\mathrm{i}}{2}\Omega_{\mathrm{Rabi}}t_0\sigma_x) = R_x(\Omega_{\mathrm{Rabi}}t_0)$. Setting the time precisely so that $\Omega_{\mathrm{Rabi}}t_0 = \pi$, we get a π pulse along x axis. Similarly, tuning the phase $\gamma = \pi/2$, we get a rotation along y axis, $\hat{U} = \exp\left(-\frac{\mathrm{i}}{2}\Omega_{\mathrm{Rabi}}t_0\sigma_y\right) = R_y(\Omega_{\mathrm{Rabi}}t_0)$.

There are two ways of implementing Z gate. The first one is virtual Z gate. Consider the case of applying two consecutive pulses. The first one forces the qubit to rotate along the x axis by θ and followed by another x-rotation by θ but with a relative phase ϕ_0 to the first pulse.[48] The total operation could be written as

$$\begin{aligned}\hat{U} &= X_{\theta}^{(\phi_0)}X_{\theta} = \exp\left\{-\frac{\mathrm{i}\theta}{2}\left[\cos(\phi_0)\sigma_x + \sin(\phi_0)\sigma_y\right]\right\}X_{\theta}\\ &= \mathrm{e}^{\mathrm{i}\frac{\phi_0}{2}\sigma_z}\mathrm{e}^{-\mathrm{i}\frac{\theta}{2}\sigma_x}\mathrm{e}^{-\mathrm{i}\frac{\phi_0}{2}\sigma_z}X_{\theta} = Z_{-\phi_0}X_{\theta}Z_{\phi_0}X_{\theta}.\end{aligned} \tag{14}$$

We can see that the total effect of phase ϕ_0 is to perform a rotation along z axis by ϕ_0. Since our readout is along the z axis, the last z-rotation does not matter. Consequently, a virtual Z gate is achieved. The other conventional method to perform Z gate is to tune the frequency of Xmon by adjusting external

flux in the SQUID of the qubit. The Hamiltonian of the Xmon could be written as

$$\hat{H} = -\frac{1}{2}\sqrt{8E_{\mathrm{C}}E_{\mathrm{J}}^{\max}\left|\cos\left(\frac{\pi\Phi_{\mathrm{ext}}}{\Phi_0}\right)\right|}\,\sigma_z = -\frac{\hbar\omega_{\mathrm{q}}'}{2}\sigma_z, \quad (15)$$

where $\omega_{\mathrm{q}}' = \sqrt{8E_{\mathrm{C}}E_{\mathrm{J}}^{\max}|\cos(\pi\Phi_{\mathrm{ext}}/\Phi_0)|}/\hbar$ is the qubit frequency that could be tuned by external flux. Thus, the evolution operator is

$$\begin{aligned}\hat{U} &= \exp\left(-\frac{\mathrm{i}}{\hbar}\int_0^{t_0}\hat{H}(t')\,\mathrm{d}t'\right) = \exp\left(-\frac{\mathrm{i}\sigma_z}{2}\int_0^{t_0}\omega_{\mathrm{q}}'(t')\,\mathrm{d}t'\right)\\ &= R_z\left(-\int_0^{t_0}\omega_{\mathrm{q}}'(t')\,\mathrm{d}t'\right). \quad (16)\end{aligned}$$

By tuning the frequency carefully, an arbitrary angle rotation along z axis could be achieved. Since any rotation on the Bloch sphere could be decomposed into 3 rotations, $R(\alpha,\beta,\gamma) = R_z(\alpha)R_y(\beta)R_z(\gamma)$, all the single qubit operations could be achieved. Moreover, the rotation can be accomplished along only two axes, which would simplify the implementation at the hardware level.[49]

2.2.2. Two qubit operations

As we know, a small gate set composed of single qubit gates and a two-qubit gate,

$$\{\mathrm{H},\mathrm{S},\mathrm{T},\mathrm{CNOT}\}, \quad (17)$$

the so-called "Clifford + T" set, is able to perform universal quantum computation.[50] In this section, we will first discuss how to perform $\sqrt{\mathrm{iSWAP}}$ gate and iSWAP gate, two important two-qubit gates in quantum computation, followed by an introduction of implementing CNOT gate based on the iSWAP gate. Controlled Z (CZ) gate, which is also denoted as controlled phase (CPHASE) gate, and cross-resonance (CR) gate are other two types of important two-qubit gates. With these gates, the universal quantum computation without error-correction could in principle be achieved.

The $\sqrt{\mathrm{iSWAP}}$ gate can be realized with two Xmon qubits, which are coupled via a capacitor or a resonator, and both of them could only do $\sigma_x\sigma_x$ or $\sigma_y\sigma_y$ but not $\sigma_z\sigma_z$ coupling. With the resonator, the coupling Hamiltonian is (using RWA)

$$\hat{H}_{\mathrm{couple}} = \hbar\frac{g^2}{\Delta}\left(\sigma_1^+\sigma_2^- + \sigma_1^-\sigma_2^+\right), \quad (18)$$

where $\Delta = \omega_{\mathrm{r}} - \omega_{\mathrm{q1}} = \omega_{\mathrm{r}} - \omega_{\mathrm{q2}}$ is the detuning between qubits and the resonator, and g^2/Δ is the effective coupling strength. With the interaction time $t_{\mathrm{int}} = \pi\Delta/2g^2$, the matrix of $\sqrt{\mathrm{iSWAP}}$ gate can be expressed as

$$\hat{U}_{\sqrt{\mathrm{iSWAP}}} = \exp\left(-\frac{\mathrm{i}}{\hbar}\int_0^{t_{\mathrm{int}}}\hat{H}_{\mathrm{couple}}\,\mathrm{d}t\right) = \begin{bmatrix}1 & 0 & 0 & 0\\ 0 & \frac{1}{\sqrt{2}} & \frac{-\mathrm{i}}{\sqrt{2}} & 0\\ 0 & \frac{-\mathrm{i}}{\sqrt{2}} & \frac{1}{\sqrt{2}} & 0\\ 0 & 0 & 0 & 1\end{bmatrix}, \quad (19)$$

which can transform a product state to an entangled state. If the interaction time is doubled, i.e., $t_{\mathrm{int}} = \pi\Delta/g^2$, one obtains the iSWAP gate, whose matrix is

$$\hat{U}_{\mathrm{iSWAP}} = \exp\left(-\frac{\mathrm{i}}{\hbar}\int_0^{t_{\mathrm{int}}}\hat{H}_{\mathrm{couple}}\,\mathrm{d}t\right) = \begin{bmatrix}1 & 0 & 0 & 0\\ 0 & 0 & -\mathrm{i} & 0\\ 0 & -\mathrm{i} & 0 & 0\\ 0 & 0 & 0 & 1\end{bmatrix}. \quad (20)$$

It swaps the excitation between two qubits with an additional phase. With some single-qubit gates and iSWAP gates, one can generate a CNOT gate,[51,52] as shown in Fig. 8.

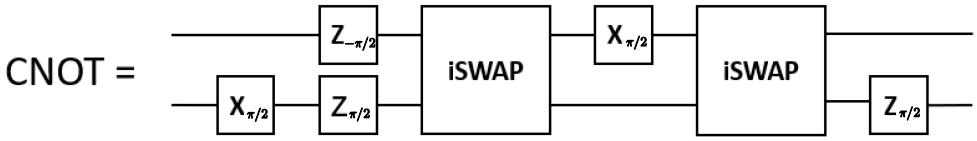


Fig. 8. CNOT gate generated from iSWAP gate.

When operating superconducting qubits only with the lowest two energy levels, higher energy levels should be avoided because they tend to deteriorate the performance of a qubit. However, for the case of transmon qubits, the higher energy levels can be used to generate CZ gates.[53] The CZ gate is often implemented by adiabatic tuning.[41,54] In recent years, some high fidelity non-adiabatic CZ gates are also realized.[55,56] Combining a CZ gate and two Hadamard gates, the CNOT gate can be generated, as shown in Fig. 9.

CR gate is an all-microwave two-qubit entangling gate for qubits whose frequencies are not tunable.[57–59] When the target qubit is applied by microwaves that are resonant with the control qubit, the coupling interaction turns on. Since such qubits are not flux-tunable, it is less sensitive to the flux noise, which leads to longer decoherence time. Combined with single-qubit gates, the CR gate can also relate to the CNOT gate.[44,58]

Table 2 summarizes the fidelities of state-of-the-art two-qubit gates of superconducting qubits.

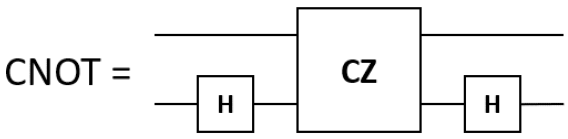


Fig. 9. CNOT gate generated from CZ gate.

Table 2. Fidelities of two-qubit gates.

Type	Qubit type	Fidelity (%)	Gate time (ns)	Method of measurement	Group	Year
CZ	Xmon	99.4	40	RB	UCSB[41]	2014
CZ (RIP)	3D transmon	98.53	413	RB	IBM[60]	2016
CZ	transmon	95	278	QPT	Regetti computing[61]	2018
CZ	Xmon	99.54	40	RB	USTC[62]	2019
CZ	transmon	99.1	40	RB	Delft UT[63]	2019
CZ	transmon	98.8	176	RB	UCBerkley[64]	2020
CZ	Xmon	99.5	30	RB	SUST[65]	2020
CZ	Xmon	99.7	60	RB	MIT[66]	2020
CR	transmon	99.1	190	RB	IBM[67]	2016
iSWAP	transmon	98.2	183	RB	IBM[68]	2016
iSWAP	transmon	94.0	135	RB	Rigetti computing[69]	2018
iSWAP	transmon	98.5	190	RB	Princeton[70]	2019
iSWAP-like	transmon	99.66	18	XEB	UCSB[56]	2019
$\sqrt{\text{iSWAP}}$	transmon	94.8	95	QPT	Princeton[70]	2019
CNOT	transmon	79	4600	QPT	Yale[71]	2018
CNOT	transmon	89	190	QPT	Yale[72]	2018
CNOT	Xmon	90.8	209	QPT	CAS[73]	2020

Annotation: (1) RB: randomized benchmarking. (2) QPT: quantum process tomography. (3) XEB: cross-entropy benchmarking.

2.3. Qubit readout

For any quantum processor, readout is expected to be fast and of high fidelity. The readout method is dependent on the measured observables. For a charge qubit, the quantum information is stored in the electric charge on the superconducting island, which could be detected by a single-electron transistor (SET).[8] For a flux qubit, the persistent current of two states is different so that dc-SQUID can be used to detect them.[74] As for a phase qubit, it is much more likely to tunnel at higher levels. After sending a probe signal which induces the excited qubit to the next states with large tunneling probability, one can distinguish the two states according to the voltage across the junction.[10,23]

When the eigenstates of the observable are also stationary states, repeated measurement would produce the same results, which provides a way to increase the fidelity of measurement. Such repeatable measurements are called quantum nondemolition (QND) measurement.[75] A QND method in superconducting quantum circuits is the dispersive readout, which is also based on the qubit–resonator coupling model.[75] While frequency of the qubit and the resonator detunes significantly, i.e., $\Delta = \omega_{\rm q} - \omega_{\rm r} \gg g$, the system is in the dispersion regime. With dispersion coupling, the Hamiltonian of the system can be effectively written as

$$\hat{H} \approx \hbar\omega_{\rm r}\left(1+\frac{g^2}{\Delta}\sigma_z\right)\hat{a}^{+}\hat{a}+\frac{1}{2}\hbar\omega_{\rm q}\sigma_z. \tag{21}$$

From the first term we know that the frequency of the resonator depends on the state of qubit now. For $|\uparrow\rangle$ state, the resonator frequency is $\omega_{\rm r}\left(1+g^2/\Delta\right)$ and for $|\downarrow\rangle$ state it is $\omega_{\rm r}\left(1-g^2/\Delta\right)$. A dispersion shift happens and thus by measuring the resonator frequency, the state of qubit could be readout. According to $\left[\hat{H},\sigma_z\right]=0$, dispersion readout is a QND measurement, which means that the measurement of the qubit does not destroy it, allowing multiple repeated measurements to improve the precision. In experiments, the signal for readout is so small that some amplifications are necessary. How to reduce extra noise introduced by amplifiers while reduce backaction on the qubit is an important topic in readout. Quantum noise limited amplifiers[76] have developed rapidly in recent years, which makes single-shot readout possible and keeps the qubit from backaction noise in the quantum limit.[77,78]

3. Superconducting quantum computing

3.1. Quantum computing without error correction

With the development of superconducting quantum computing device, some simple versions of quantum algorithms have already been implemented in real systems, providing practical demonstrations that a quantum computer can be fulfilled and have become fundamental step for further investigation.

Deutsch algorithm is the first proposed quantum algorithm.[79] Deutsch–Jozsa (D-J) algorithm is its improved version showing the advantages of quantum algorithm from making use of superposition states.[80] In 2009, Deutsch–Jozsa algorithm was performed in a two-transmon-qubit superconducting quantum processor by DiCarlo *et al.*, and Grover algorithm was also performed in real machine for the first time.[81]

Proposed in 1994 by Peter Shor, Shor algorithm is aimed to compute prime factors for composite numbers for much shorter time than all classical algorithms do.[82] And since 1994, it has been regarded as a deadly threat to RSA protocol, whose ability of maintaining secrecy is dependent on the difficulty of factorizing big composite numbers.

Here is a brief description for Shor algorithm.[82] The problem of factorizing a large number N can be converted to

the problem of finding r, the order in the multiplicative group of a random integer a, that is, $a^r = 1 (\mathrm{mod}\, N)$. Here, a is relatively prime to and smaller than N. If r is not an odd number or $a = -1 (\mathrm{mod}\, N)$, then a should be replaced by another random integer and r should be calculated correspondingly again. With Euclid algorithm, it is easy to find the greatest common divisors of $a^{r/2} \pm 1$ and N, $\gcd(a^{r/2} \pm 1, N)$, as the prime factors of N. The order r equals the period of the function $f_{a,N}(x)$,

$$f_{a,N}(x) = a^x (\mathrm{mod}\, N), \tag{22}$$

which needs an operation called modular exponentiation. In quantum circuits, modular exponentiations for calculating $f_{a,N}(x)$ can be reduced to modular multiplications, which can be further reduced to modular additions. And modular additions can be realized with CNOT and Toffoli gates. To calculate the order r, two registers both consisting of L qubits are required. L should be chosen with inequalities $2N^2 \leq 2^L \leq 4N^2$. The input x is stored in register 1, and the output $f_{a,N}(x)$ is stored in register 2. At the beginning of quantum circuits for finding the order r, Hadamard gates are applied to every qubit in register 1, thus making superposition of states from $|0\rangle$ to $|2^L - 1\rangle$:

$$|\Phi_1\rangle = |0\rangle \rightarrow |\Phi_1\rangle = \frac{1}{\sqrt{2^L}} \sum_{x=0}^{2^L-1} |x\rangle, \tag{23}$$

where $|\Phi_1\rangle$ represents the state of qubits in register 1. After modular exponentiation, the outputs of function from $f_{a,N}(0)$ to $f_{a,N}(2^L - 1)$ are stored in the entangled states of qubits in register 2:

$$\begin{aligned} |\Phi\rangle &= \frac{1}{\sqrt{2^L}} \sum_{x=0}^{2^L-1} |x\rangle |0\rangle \\ \rightarrow |\Phi\rangle &= \frac{1}{\sqrt{2^L}} \sum_{x=0}^{2^L-1} |x\rangle |a^x (\mathrm{mod}\, N)\rangle, \end{aligned} \tag{24}$$

where $|\Phi\rangle$ denotes the state of all qubits. Then apply quantum Fourier transform to register 1, the two registers will be left in the state

$$|\Phi\rangle = \frac{1}{2^L} \sum_{x=0}^{2^L-1} \exp\left(2\pi \mathrm{i} xy/2^L\right) |y\rangle |a^x (\mathrm{mod}\, N)\rangle. \tag{25}$$

Finally, the value of y of register 1 is measured. With strict analysis in literature,[82] there is

$$\left| \frac{y}{2^L} - \frac{k}{r} \right| \leq \frac{1}{2 \cdot 2^L}, \tag{26}$$

where k is an integer. The fraction k/r can be obtained in lowest terms by rounding $y/2^L$ to the nearest fraction whose denominator is smaller than N. This can be done with a continued fraction expansion of $y/2^L$. By repeating steps above for $O(\log\log r)$ times, the correct r can be obtained with a high possibility.[82] Another version of Shor algorithm was proposed by Zalka.[83] Researchers have begun to try Shor algorithm for factorizing small numbers in experiments. In 2012, Martinis' group computed prime factors of 15 with a quantum processor consisting of 4 Josephson phase qubits.[84]

In 2009, Harrow–Hassidim–Lloyd algorithm (HHL) was proposed to solve linear systems of equations.[85] Usually the formalism of this problem is $\boldsymbol{A}\boldsymbol{x} = \boldsymbol{b}$, where $\boldsymbol{x}$ is unknown while $\boldsymbol{A}$ and $\boldsymbol{b}$ are given. HHL has been changed into many different versions combining classical and quantum algorithm components. Recently, Chen *et al.*[86] presented a hybrid classical-quantum linear solver working in a NISQ quantum computer for handling situations with the matrix $\boldsymbol{A}$ useful for Markov decision problems, such as reinforcement learning. Using classical computer to perform ancilla quantum encoding (AQE) of HHL, Lee *et al.* modified the original HHL algorithm and realized this hybrid HHL algorithm on IBM Quantum Experience (IBMQX).[87] The same results as that of original HHL were obtained and the depth of the quantum circuit was reduced, showing that hybrid algorithms are possible to be more resource-saving than pure quantum algorithms are.

Quantum approximate optimization algorithm (QAOA) was proposed by Farhi *et al.* in 2014.[88] QAOA is aimed to solve combinatorial optimization problems which belong to NP-hard problems difficult to solve with classical computers when inputs are large. Unlike sampling problems,[2] combinatorial optimization problems are more practical. Therefore, QAOA has potential to realize quantum supremacy and at the same time to solve some practical problems in the production and service. However, performing simulations of QAOA, Guerreschi *et al.* pointed out that quantum speedup would not be realized until the quantum computer with several hundreds of qubits is available.[89] Up to now, quantum supremacy demonstrated with QAOA has yet been implemented.

3.2. Error correction

In a classical computer, errors mean undesirable bit flips. However, errors in a quantum computer are beyond this situation, including X error and Z error, caused by erroneous gate operations or qubit decoherence. X error changes the probability of measurement results, $|0\rangle$ or $|1\rangle$ (bit-flip error), and Z error changes the relative phase between $|0\rangle$ and $|1\rangle$ (phase-flip error). Leakage, another important kind of error, means qubits leave the computational subspace.

An error rate is defined as the probability that an error appears on a qubit after a gate operation. And a gate fidelity, ranging from 0 to 1, represents the difference between the qubit state prepared by a gate and the ideal qubit state that

one wants. To characterize errors produced during computation, researchers developed several experimental methods of measuring gate fidelities.

3.2.1. Error characterization

Error characterization methods, which are still being developed, include quantum process tomography (QPT)[90] and randomized benchmarking (RB).[91]

QPT was proposed the earliest. For a d-dimension Hilbert space of a series of qubits, QPT requires d^2 input states and d^4 measurements, which produces a lot of data that need much time to analyze. Recently, Hou *el al.* provided a new self-guided algorithm for QPT, achieving $1/n$ scaling when the unknown process is used for n times, which has the same effect as that of traditional QPT.[92]

The research on RB is now focusing on realization of multi-qubit RB. Mcday *et al.*[93] used three fixed-frequency transmons to perform RB and measured the three-qubit error per Clifford (EPC). By introducing certain coherent errors to the gates, three-qubit error was increased but could not be predicted precisely by simultaneous one- and two-qubit RB. Helsen *et al.*[94] brought a theoretical analysis that much fewer sampled sequences can reach the requirement of RB than that of standard RB. The required number of sampled sequences scales with the average error rate, but is not mainly dependent on the number of qubits.

If errors in different qubits are statistically independent and the error rate is lower than a threshold, it is possible to run a quantum program for arbitrary long time with error-correcting codes, even though the error-correcting gates bring errors. This has been proved by the threshold theorem.[95]

3.2.2. Early error-correcting codes

Error-correcting codes based on classical linear codes developed by Shor, Calderbank, and Steane were classified as Calderbank–Shor–Steane codes (CSS),[96–98] which were found to be a subset of a class of more general codes called stabilizer codes.[98,99] With the development of quantum computing devices, researchers found it difficult to utilize these codes in real machines because of restrict requirement of both accuracy thresholds and good connectivity between qubits. Therefore, surface codes and bosonic codes were proposed as more suitable and alternative schemes.

3.2.3. Surface codes

Surface codes were derived by Kitaev from toric codes.[100] Wang *et al.* came up with a better decoding algorithm for Kitaev surface codes, which can improve the threshold error rate to over 1%.[101] The algorithm requires that qubits are arranged in a 2D square lattice and are divided in two classes. One is called data qubit and the other is called syndrome qubit. Syndrome qubits identify errors of data qubits so that the measurement results affected by these errors can be corrected. In 2012, Fowler *et al.* provided a more practical version of surface codes which could be implemented with Xmon qubits[102] and described a way of constructing logical qubits with physical qubits. The structure of the surface codes is shown in Fig. 10. Here syndrome qubits are called measurement qubits, consisting of measure-Z qubits and measure-X qubits. Measurement qubits detect Z errors and X errors of data qubits around them. The implementation methods of single-qubit gates including Hadamard, S, and T and two-qubit gate like CNOT for logical qubits were also introduced in the literature,[102] which showed the possibility of building a universal quantum computer with surface codes.

Ghosh *et al.* studied the leakage in a two-qubit superconducting stabilizer measurement circuit and supplied two solutions: (a) using stabilizer-based topological error-correcting codes for qudits; (b) repeatedly initializing, operating, and measuring each qubit as additional steps of the standard topological error correction.[103]

Recently, Natalie *et al.*[104] investigated the influences of data leakage and ancilla (syndrome) leakage separately, showing two ways of maintaining the effectiveness of surface codes: confining leakage to data qubits and eliminating ancilla qubit leakage at the critical fault location.

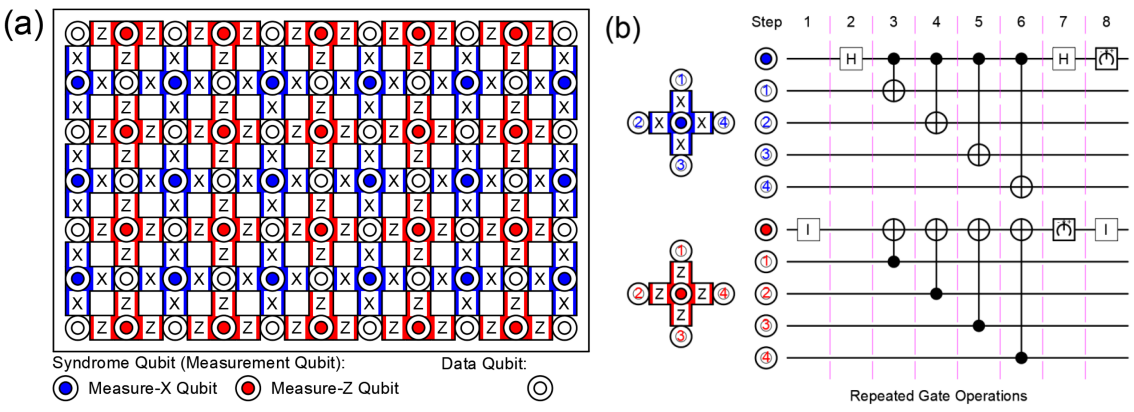


Fig. 10. Schematic of circuits for realizing surface codes. (a) A 2D array implementation of surface codes. (b) Geometric sequences of operations (left), and quantum circuit (right) for one surface code cycle for a measure-X qubit and a measure-Z qubit.

The physical implementation of surface codes began in 2014.[105] Kelly *et al.* performed an experiment of protecting classical states from environment-induced bit-flip errors, with 9 Xmon qubits (4 measurement qubits and 5 data qubits) manufactured and arranged in a line alternately, forming a 1D surface codes architecture which was called repetition code.[105] The crisscross-like capacitors of Xmon qubits, coupling with neighbor capacitors for two-qubit gate operations, enable the architecture of surface codes to expand to a larger scale.

In 2017, Takita *et al.*[106] demonstrated fault-tolerant state preparation in a superconducting circuit with five transmon qubits which constitutes the smallest surface code architecture, as shown in Fig. 11.

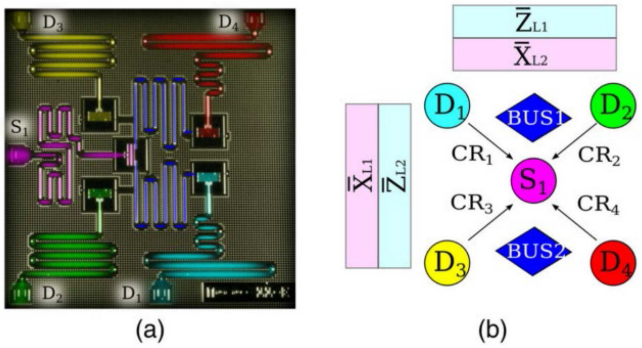


Fig. 11. (a) False-colored micrograph of five transmon qubits. (b) Cartoon representation of a five-qubit lattice and the logical operators on the data qubits.[106]

Recently, using a superconducting circuit of surface codes consisting of seven transmon qubits (4 data qubits, 2 Z-type ancilla qubits, and 1 X-type ancilla qubit), Andersen *et al.* prepared logical states $|0\rangle_L$, $|1\rangle_L$, $|+\rangle_L$, and $|-\rangle_L$ of the encoded logical qubit.[107]

The main idea of surface codes is enlarging the number of physical qubits, so that logical qubits can be encoded in a Hilbert space with a large number of dimensions. However, with the increasing number of physical qubits, the noise channels increase proportionally. And non-localized multi-body interactions between physical qubits will make the control system and manipulation very complicated.

3.2.4. Bosonic quantum codes

Instead of obtaining a huge Hilbert space for encoding by adding many physical qubits, bosonic quantum codes, proposed in 1997,[108,109] make use of the infinite-dimensional Hilbert space spanned by energy eigenstates of a single quantum harmonic oscillator (bosonic modes) for encoding, reducing the requirement for hardware.

Mirrahimi *et al.*[110] proposed a paradigm of error correction by encoding quantum information in a quantum harmonic oscillator made of a cavity. These schemes required two- or four-component Schrödinger cat states as the logical qubit, which is called the cat codes. Wang *et al.*[111] realized a two-mode cat state of electromagnetic fields in two superconducting cavities, which had a strong dispersive interaction with an artificial atom made from Josephson junction. Rosenblum *et al.*[112] performed a CNOT gate between multiphoton qubits encoded in two cavities by coupling them to an RF-driven ancilla transmon, which is helpful for meeting the challenge of fast interaction between the two cavities without large nonlinearities and decoherence from the ancillary element.

Hu *et al.* demonstrated the experiment of another kind of bosonic quantum codes, called binomial bosonic code.[113] The logical qubit was operated with universal quantum gate set with 97% average process fidelity and had a lifetime 2.8 times longer than that of uncorrected case. Recently, Ma *et al.*[114] extended the error-transparent (ET) gates to the bosonic binomial code, which could tolerate errors occurred on the logical gates. The gate Hamiltonians of ET gates were designed by photon-number-resolved AC Stark shifts.

4. Superconducting quantum simulation

Quantum simulation was first proposed by Feynman *et al.* in the 1980s,[115] to solve some quantum problems that would require exponentially increasing resources on classical computers with scale, which makes them intractable classically. Intuitively, quantum problems need quantum technology to deal with.[116] After decades of hard work, quantum simulation has made great progress and is expected to be applied in practical applications in the near future.[1,117]

4.1. Digital and analog quantum simulation

Quantum simulation takes a controllable quantum device to simulate other complex quantum system that is difficult to directly study and control.[3,118] The basic schematic is depicted in Fig. 12. The initial state $|\Psi(0)\rangle$ of the quantum system and the time evolution operator, $\hat{U}$, are mapped to the quantum simulator $|\psi(0)\rangle$ and $\hat{U}'$. After the evolution, the result of the simulator $|\psi(t)\rangle$ is mapped back to the quantum system to obtain the required information. With quantum device, computational resources would not scale exponentially. Because of the relatively simple preparation, high degree of freedom in manipulation, high readout efficiency, tunable qubit frequency, coupling strength, superconducting quantum circuits have great advantages in quantum simulation. Moreover, since the particles in superconducting qubits are the excited states of the circuits but not physical particles, they need not obey the conservation law of particle number, which allows the simulation of non-equilibrium phenomena.[119–121] Generally, there are two types of quantum simulations, digital quantum simulation (DQS) and analog quantum simulation (AQS).[3,122]

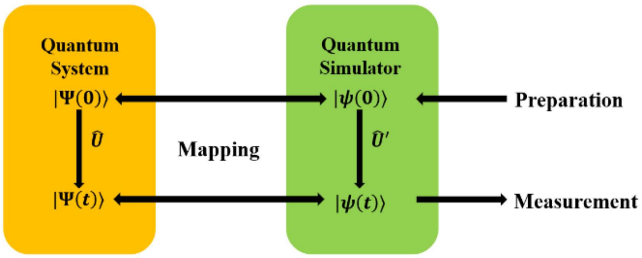


Fig. 12. Quantum simulation.

4.1.1. Digital quantum simulation

Digital quantum simulation decomposes the complex dynamic evolution operator $\hat{U}$ of the simulated system into a series of single-qubit or two-qubit gates that can be realized by quantum device.[117] Such a scheme is compatible with universal quantum computers with error correction. It does not mean that DQS is completely "universal". In fact, there are some systems that DQS cannot effectively simulate.[3] In principle, DQS can effectively simulate any system whose Hamiltonian is finite-dimensional and local, but ineffectively for other problems. Fortunately, most of the interesting quantum systems have finite-dimensional local Hamiltonian. Therefore, DQS can effectively solve these problems. Generally, DQS includes three steps: initial state preparation, unitary evolution, and final state measurement.

Initial state preparation It is crucial to prepare a good initial state for DQS, which affects the accuracy of the evolution result and the efficiency of the simulation. However, most initial states of practical systems are quite complicated or even unknown, so the preparation of initial states is a tough problem.[123,124] Fortunately, there are some efficient preparation methods for specific problems. For example, for the case that the initial state is a specified pure state, direct preparation is a valid method.[125]

Unitary evolution The decomposition of unitary evolution operator is the core step of DQS.[3,126] Considering only the local interaction, the Hamiltonian of the system can be written as

$$\hat{H} = \sum_{l=1}^{M} \hat{H}_l, \tag{27}$$

where $\hat{H}_l$ acts on at most a constant c number of systems. Since $\hat{H}_l$ and $\hat{H}_{l'}$ do not commute in most cases, it is difficult to decompose the time evolution into simple forms such as $\hat{U} = \prod_l \exp(-\mathrm{i}\hat{H}_l t/\hbar)$. The Lie–Trotter–Suzuki decomposition is commonly employed to deal with these unitary operators, which breaks the evolution time into many small time steps with a duration of Δt,

$$\hat{U} = \left[\exp\left(-\frac{\mathrm{i}\hat{H}\Delta t}{\hbar}\right)\right]^{\frac{t}{\Delta t}}. \tag{28}$$

In this way, the simulator evolves gradually to approximate the actual dynamic behavior of the quantum system. Using the first-order Trotter formula,[127,128] it can be written as

$$\begin{aligned}\hat{U}(\Delta t) &= \exp\left(-\frac{\mathrm{i}}{\hbar}\sum_{l=1}^{M}\hat{H}_l\Delta t\right)\\ &= \prod_{l=1}^{M}\exp\left(-\frac{\mathrm{i}}{\hbar}\hat{H}_l\Delta t\right) + O\left((\Delta t)^2\right).\end{aligned} \tag{29}$$

When $\Delta t \to 0$, there is

$$\hat{U}(\Delta t) \approx \prod_{l=1}^{M}\exp\left(-\frac{\mathrm{i}}{\hbar}\hat{H}_l\Delta t\right), \tag{30}$$

which is close to the actual evolution result of the original quantum system. To acquire more precision, higher-order Trotter formulas could be implemented, though it is much more complicated.

The scale of gate circuits is related to the problem and the specific characteristics of the simulator. Since $\left[\hat{U},\hat{U}'\right] = 0$ is not strictly hold, there will always be errors between the simulation results and the actual behavior. The accuracy can be improved by increasing the number of evolution steps. Intuitively, increasing the number of steps will not lead to a longer evolution time, because the duration of each step also gets shorter such that the total simulation time remains unchanged. However, the number of quantum gates required by DQS will scale with the accuracy dramatically, which makes simulator too large to implement physically. In addition, research by Clark *et al.*[129] showed that the accuracy will also seriously affect the total run time of the simulation. The simulation time will grow exponentially with desired accuracy.

Measurement The last step of DQS is measurement, in which the desired information is obtained from the evolution result. Due to the characteristics of quantum measurement, all the information of the final state could not be extracted in one measurement. In principle, it is possible to obtain all the information in the final state with QST, but it will consume a lot of resources and thus seriously affect the efficiency of quantum simulation. For a given problem, extracting some quantities, such as correlation functions, operator spectrum, and so on, of a given state, and discarding some unwanted redundant information are much more practical, which improves measurement efficiency while obtaining effective information.[130]

4.1.2. Analog quantum simulation

Unlike digital quantum simulation, analog quantum simulation (AQS) does not decompose the evolution operator into many small steps, it directly maps the Hamiltonian of the quantum system to the simulator, taking advantage of their physical similarity. One can get some intuition of AQS with its classical counterpart: the analog classical simulation (ACS),

which has been studied a lot in 20th century before rapid development of classical computers. A good example for ACS is to simulate a simple pendulum with an LC circuit. By observing the influence of circuit parameters on the input and output characteristics of the system, the relationship between the pendulum parameters and its dynamic behavior can be understood. Physical similarity of the two systems is utilized in this example. Since analog simulation requires a certain similarity of physical characteristics between the quantum system and the simulator, it is not universal. What physical system can be effectively simulated depends on the characteristics of the problem and the structure of the simulator.

A great advantage of AQS is that it is more efficient on the specific problems, and has less requirements on the physical characteristics of the simulator, such as the decoherence time of qubits. This feature allows AQS to operate effectively without error correction. Although it might be unable to achieve high accuracy, it is sufficient to obtain some results with less precision or certain qualitative conclusions. Therefore, AQS will be an important subject in the NISQ era, and it is expected that quantum simulation will demonstrate the advantages of quantum computers in practical applications before the implementation of universal quantum computers.[1,131]

The construction of the evolution operator corresponding to the simulated system on quantum simulator is simple for some systems, but sometimes it may also be rather complicated, requiring the participation of many auxiliary qubits or other structures. There is no universal method for this subject so far. In AQS, the initial state preparation is relatively simple, which in most cases can be prepared by relaxation. Due to the similarity between the target system and the quantum simulator, the readout of the final state is not complicated as well. It is generally sufficient to readout directly. In such procedures it is more efficient than DQS. One could also note that it is not always necessary to simulate the entire quantum system. To simulate part of dynamic behavior of the system is also sufficient in some cases. The rest can be done on a classical computer. It can also be combined with DQS to form digital-analog quantum simulation, making full use of the advantages of both methods, such as flexibility and efficiency.[132] The benchmarking of an analog quantum simulator remains an open question. A heuristic idea is to take some tasks that could be tackled with classical computers to be the benchmark.

4.2. Applications

Quantum simulators can solve some problems that are difficult to solve in classical calculations and experiments, having important applications in physics, chemistry, and biology. It has brought results that were previously difficult to obtain in many fields and will allow testing of some theoretical models. In addition, quantum simulation itself is a good platform for further study into quantum phenomena. In following sections we will introduce some applications of quantum simulation in some problems where superconducting qubits have shown their unique role, including Hubbard model, topological properties, open quantum system, quantum chemistry calculation, etc.

4.2.1. Hubbard model

Hubbard model is a highly general model in condensed matter physics, which describes the on-site interacting particles on a lattice. The Hubbard Hamiltonian takes the form[133]

$$\hat{H} = -t\sum_{\langle i,j\rangle,\sigma}\left(\hat{c}^{+}_{i,\sigma}\hat{c}_{j,\sigma}+\hat{c}^{+}_{j,\sigma}\hat{c}_{i,\sigma}\right)+U\sum_{j}\hat{n}_{j\uparrow}\hat{n}_{j\downarrow}, \quad (31)$$

where t parametrizes the "kinetic-energy", and U is the on-site repulsion potential energy. The first term describes the near-neighbor hopping of a tight-binding model and the second term denotes the potential energy cost if two particles occupy a site. It seems simple, but for models more than one dimension with large number of particles, it is too difficult to treat classically.

Quantum simulation plays an important role in solving such problems. Las Heras *et al.*[134] proposed an implementation of the Fermi–Hubbard models with DQS, which consists of Jordan–Wigner mapping, Trotter decomposition, and multi-qubit gates. This paved the way for simulating complex fermionic dynamics with superconducting circuits, which was experimentally validated by Barends *et al.* latter.[135] Dallaire-Demers *et al.* proposed a hybrid quantum-classical approach to Fermi–Hubbard model and found out that the Trotter–Suzuki errors can be made as small as possible.[136] They also pointed out that thermodynamic properties of a complex fermionic lattice which are inaccessible for classical computers could be simulated in a quantum computer with a few tens of qubits.[137] Reiner *et al.* showed how to simulate the one-dimensional Fermi–Hubbard model with a double chains of transmon qubits and proposed protocols for gaining confidence in the results of simulation.[138] According to Cai's estimation,[139] it would be possible to implement a 50-qubit Hubbard model variational quantum eigensolver (VQE) in the NISQ era.

Except for Fermi–Hubbard model, Bose–Hubbard models have also been studied with superconducting quantum simulator. Roushan *et al.* implemented a technique for resolving the energy levels of interacting photons and benchmarked it by capturing the main feature of the intricate energy spectrum with a nine-qubit chain.[140] Ma *et al.* built a Bose–Hubbard lattice for photons in strongly interacting regime to explore strongly correlated quantum matter, showing the power of superconducting quantum simulator in this field.[141] The above results are for 1D Bose–Hubbard models,

which can also be solved by analytical methods.[142] Yanay *et al.* have proposed a scheme for implementation of the two-dimension hard-core Bose–Hubbard model with an array of floating transmon qubits.[143] Ye *et al.* constructed a Bose–Hubbard ladder of 20 qubits on a 24-qubit superconducting processor, showing the way to simulate exotic logic particles by subtly encoding physical qubits.[144] Motivated by the quantum simulation on a ladder circuit, Li *et al.* found out that in the hard-core limit, the rung-pair localization can exist both at the edges and in the bulk, and the system can display a localization similar to the many-body localization.[145]

4.2.2. Topological properties

In condensed-matter physics, topology is an important fundamental concept. In recent years, searching topological states with superconducting qubits becomes a field of growing interest. It provides a powerful platform to research topological phenomena in physics which is difficult to study directly. In 2014, Roushan *et al.* investigated the topological properties of several quantum systems with a superconducting quantum circuit.[146] They have shown the power of the method in interacting quantum systems, discovering the emergence of a topological phase induced by interaction. From a superconducting qubit, Schroer *et al.* also observed a topological transition.[147] By mapping the momentum space of condensed matter to the controllable parameter space of superconducting quantum circuits, Tan *et al.* imaged a tunable gapless band structure which is typical of topological semimetals, and manipulated two topological quantum phase transitions.[148] In the latter works, they have observed the Maxwell points in the Maxwell metal bands, and Weyl points in Weyl-semimetal bands. Both the band structures can be manipulated.[149,150] In a one-dimension qubit chain, Cai *et al.* have measured the topological winding numbers and caught the phenomenon of topological magnon insulator states.[151] In 2020, the topological property of two-dimensional superconducting circuit was investigated.[152]

4.2.3. Open quantum system

In quantum computation, decoherence of qubits is what everyone tries to mitigate. However, it can also be exploited to study open quantum systems due to their similarity. In classical computation, it is much more difficult to simulate the dynamics of open quantum systems than closed quantum systems since the Lindblad equation requires more resources to solve than Schrödinger equation. Lloyd suggested that one can utilize the natural decoherence of quantum simulator to simulate open quantum systems.[116] In superconducting quantum simulator, open systems can also be described by the spin boson model.[153,155] In most cases, the spin–boson model that consists of a single two-level system coupled to bosonic modes could be directly mapped to superconducting qubits and resonators. It is possible for classical simulation to solve the problem in the limit of weak coupling, but impossible for strong coupling, which requires quantum simulation. Such model has provided a platform to reveal the complex quantum dynamics in the ultra-strong coupling (USC) regime.[156–158] Experiments have shown that the quantum Rabi Hamiltonian in USC regime could be simulated in superconducting quantum simulator, allowing the implementation of nonlinear process in which the number of excitations does not conserve. It also provided new avenues for nonlinear optics, concerning metamaterial,[159,160] phase transition,[161,162] and so on.

4.2.4. Quantum chemistry

Quantum computation and quantum simulation are also prompted by chemistry, since large scale exact first-principles calculations of molecular properties are intractable in classical computers.[124,163,164] Owing to the computational complexity, classical methods for chemistry simulation utilize many approximation techniques, trying to avoid explicitly describing the full many-body wave function and their propagation in time in a computation. However, such features could be implemented well in a quantum computer.

For static problems in quantum chemistry, a method based on the time-independent variational principle, VQE, is useful.[165,166] With VQE, it is possible to simulate the ground states of quantum systems. O'Malley *et al.* are the first to report an electronic structure performed on a quantum computer with VQE and the canonical quantum algorithm for chemistry, computing the surface energy of H_2. They found that the VQE is robust to certain errors.[167] Colless *et al.* applied quantum subspace expansion approach to the H_2 on a superconducting quantum chip, extracting both ground and excited states.[168] Kandala *et al.* computed the ground-state energy for BeH_2, whose size is much larger, on an experiment with up to six qubits.[169] This was the largest size in quantum simulations of chemistry before the simulation of isomerization mechanism of diazene implemented by Google AI Quantum ad Collaborators, using one dozen qubits.[170] One could see that quantum chemistry developed rapidly in recent years and it is expected to further demonstrate its ability in the NISQ era.

4.2.5. Other applications

Since quantum mechanics plays a fundamental role in modern physics, there are many other applications in quantum simulation. For example, Pedernales *et al.*[171] showed that the dynamics of the Dirac equation and Klein paradox can be simulated on a superconducting qubit system, connecting relativistic quantum physics and circuit QED. Mei *et al.*[172] proposed a superconducting quantum simulator for the Holstein molecular-crystal model, opening avenues to study the electron–photon physics. Guo *et al.* observed

a dynamical quantum phase transition in a simulation of the quantum-quench dynamics of many-body systems.[173] Xu *et al.* investigated the dynamical phase transition in the Lipkin–Meshkov–Glick model, showing that superconducting quantum simulation is useful for nonequilibrium quantum many-body systems.[121] Guo *et al.* proposed an energy-resolved many-body localization transition using a 19-superconducting-qubit processor, opening a route for the experimental research of many-body mobility edges.[174]

4.3. Quantum annealing

Quantum annealing (QA), developed from classical simulated annealing (CA), is designed to solve classical combinatorial optimization problems,[1,175,176] which have important applications in classification problems,[177] machine learning,[178] quantum chemistry,[179] and high-energy physics.[180,181]

The goal of optimization problems is to find the global minimum value of the cost function. However, there are usually a large number of local minima in the landscape of the cost function, which interfere the search of solutions. Thus, the combinatorial optimization problems are usually too complicated to solve directly. To deal with such problems, classical annealing uses a heuristic method to search for the global minima. As we know, the arrangement of the solid material is not always in the lowest energy state, but trapped in a metastable state. Annealing is applied to relax the material to its most stable state, i.e., the ground state. With thermal disturbance, it can temporarily deviate from the local minima and then surpass the potential barrier to search the entire energy landscape for the minimum value. Another important step is to reduce the thermal disturbance slowly, and finally stabilize the state at the global minimum. Quantum annealing solves the problem in a similar way.

In quantum annealing, quantum fluctuation plays the role of thermal fluctuation in classical annealing. Systems are disturbed by quantum fluctuation and tunnel across the potential barrier, but not surpass it, which lead the system to converge to the global ground state more efficiently than classical annealing in some problems.

Assuming that the Hamiltonian of the system to be dealt with is $\hat{H}_0$ and the Hamiltonian associated with the external field is $\hat{H}_1$, the total time-dependent Hamiltonian can be written as[182]

$$\hat{H} = A(t)\hat{H}_0 + B(t)\hat{H}_1, \tag{32}$$

where $B(t)$ would gradually decrease from $B(0) = 1$ at first to $B(\tau) = 0$, with τ to be the computation time, while $A(t)$ would gradually increase from $A(0) = 0$ initially to $A(\tau) = 1$ at last. In this process, the system is initialized in the ground state of $\hat{H}_1$, which is easy to prepare experimentally, and then slowly transits to the ground state of $\hat{H}_0$, obtaining the required solution.

Without loss of generality, the transverse-field Ising model is a good example for quantum annealing, which has been experimentally realized with superconducting flux qubits.[183] The Hamiltonian of the device is

$$\hat{H}(t) = \Lambda(t)\hat{H}_{\rm p} + \Gamma(t)\sum_{i=1}^{N}\Delta_i\sigma_i^x, \tag{33}$$

$$\hat{H}_{\rm p} = \sum_{i=1}^{N}h_i\sigma_i^z + \sum_{i,j=1}^{N}J_{ij}\sigma_i^z\sigma_{\rm j}^z, \tag{34}$$

where $\hat{H}_{\rm p}$ denotes the Hamiltonian of the Ising model, and σ_i^z is the Pauli spin matrix for spin i, $2h_i$ is the energy bias which can be tuned by flux though the qubit, $2J_{ij}$ is the coupling energy between spins i and j. $\sum_{i=1}^{N}\Delta_i\sigma_i^x$ is the transverse term and Δ_i parameterizes the quantum tunneling. With $\Gamma(t)$ decreasing from one to zero adiabatically, $\Lambda(t)$ increases to one, resulting in the final Ising Hamiltonian and the problem is solved.

In 2011, D-wave released the first commercially available quantum annealing device,[183] and since then, a lot of proof-of-principle experiments have been realized. With 1800 *in situ* programmable superconducting niobium flux qubits, King *et al.* demonstrated a large quantum simulation of a Kosterlitz–Thouless phase transition.[184] Harris *et al.* observed phase transitions between the paramagnetic, antiferromagnetic, and spin-glass phases with a 3D $8\times8\times8$ model of interacting Ising spins.[185] Jiang *et al.* proposed a framework for integer factorization problem by converting them to an executable Ising model.[186]

However, there is always a scientific debate on whether annealing devices can actually offer a speedup over classical computers.[176] Rønnow *et al.* proposed a method on how to define and measure quantum speedup. In their experiment, they did not find evidence for the speedup.[182] Albash and Lidar demonstrated the first example showing that the experimental quantum annealer has scaling advantage over classical simulated annealing with 95% confidence. However, it does not mean that it achieves a quantum speedup either.[187] There is some other discussion on this question.[188,189]

5. Challenges and perspectives

Error correction has been the core issue of the current stage of quantum computer implementation. However, scaling qubits should also be considered simultaneously. Nowadays articles about error correction are still focusing on looking for and implementing suitable error-correcting codes based on well-made qubits, but few of them notice that the yield of qubits is also significant for scaling quantum computer. Whether the randomly-distributed invalidated qubits are able to weaken the efficiency of surface codes, and how to improve the reliability of qubits and surface codes remain unsolved. Vedral *et al.* showed that the total number of qubits required

for factorizing a big number N is $7n+1$, where n is the number of bits used to encode N.[190] Therefore, in order to factor a big number with 2048 bits, at least 14337 logical qubits are required. Assuming that we need about 4000 physical qubits to build a logical qubit, the algorithm requires 57348000 physical qubits, which has the order of magnitude around 10^7–10^8. Therefore, there is still a long period of time away from the date of breaking RSA2048 protocol, and error correction must be an unavoidable task.

Another challenge is improving synchronization and accuracy of gate operations. With millions of qubits in the same superconducting circuits, the quantum computer should be able to perform millions of accurate gate operations at the same moment, which requires high-speed, high-accuracy, and low-latency classical control modules.

There are still many unresolved problems in quantum simulation. In digital quantum simulation, it is a challenge to efficiently prepare the initial state. In terms of decomposing evolution operators, one needs to find a more efficient method that could minimize the required quantum gates while improving accuracy. For analog quantum simulation, how to benchmark the efficiency of the simulator is still an open question. Quantum annealing has shown its ability to surpass classical simulated annealing in some cases, but the question that whether it can in fact achieve quantum speed-up needs more detailed studies.

In summary, this review recalls the fundamentals of superconducting qubits and describes the progresses of quantum computing and quantum simulation, showing that many problems are still waiting for solutions. Error correction is required for universal quantum computers. Surface codes are the hopeful candidates for building large-scale quantum computers but need to be improved by tackling obstacles like leakage of qubits and qubit yield. Bosonic quantum codes could be developed further. As for quantum simulation, more practical applications of simulations are expected. Digital quantum simulation is compatible with the universal quantum computation, while analog quantum simulation is a much more unique framework which depends on the feature of physical realization. The experiments in the last two decades have been showing that superconducting qubits with circuit-QED architecture are promising physical systems for the realization of quantum computation and quantum simulation.

References

[1] Preskill J 2018 *Quantum* **2** 79
[2] Arute F, Arya K, Babbush R, *et al.* 2019 *Nature* **574** 505
[3] Martinis J M 2009 *Quantum Inf. Process* **8** 81
[4] Devoret M H and Martinis J M 2004 *Implementing Qubits with Superconducting Integrated Circuits* (Boston: Springer) pp. 163–203
[5] Devoret M H 1995 *Quantum fluctuations in electrical circuits* (Amsterdam: Elsevier) p. 351
[6] Vool U and Devoret M H 2017 *Int. J. Circ. Theor. App.* **45** 897
[7] Bouchiat V, Vion D, Joyez P, Esteve D and Devoret M H 1998 *Physica Scripta* **76** 165
[8] Nakamura Y, Pashkin Y A and Tsai J S 1999 *Nature* **398** 786
[9] Cottet A, Vion D, Aassime A, Joyez P, Esteve D and Devoret M H 2002 *Physica C* **367** 197
[10] Vion D, Aassime A, Cottet A, Joyez P, Pothier H, Urbina C, Esteve D and Devoret M H 2002 *Science* **296** 886
[11] Koch J, Yu T M, Gambetta J, Houck A A, Schuster D I, Majer J, Blais A, Devoret M H, Girvin S M and Schoelkopf R J 2007 *Phys. Rev. A* **76** 042319
[12] Barends R, Kelly J, Megrant A, Sank D, Jeffrey E, Chen Y, Yin Y, Chiaro B, Mutus J, Neill C, O'Malley P, Roushan P, Wenner J, White T C, Cleland A N and Martinis J M 2013 *Phys. Rev. Lett.* **111** 080502
[13] Chen Y, Neill C, Roushan P, *et al.* 2014 *Phys. Rev. Lett.* **113** 220502
[14] Geller M R, Donate E, Chen Y, Neill C, Roushan P and Martinis J M 2015 *Phys. Rev. A* **92** 012320
[15] Han S, Rouse R and Lukens J E 2000 *Phys. Rev. Lett.* **84** 1300
[16] Orlando T P, Mooij J E, Tian L, van der Wal C H, Levitov L S, Lloyd S and Mazo J J 1999 *Phys. Rev. B* **60** 15398
[17] Mooij J E, Orlando T P, Levitov L, Tian L, van der Wal C H and Lloyd S 1999 *Science* **285** 1036
[18] Yan F, Gustavsson S, Kamal A, Birenbaum J, Sears A P, Hover D, Gudmundsen T J, Rosenberg D, Samach G, Weber S, Yoder J L, Orlando T P, Clarke J, Kerman A J and Oliver W D 2016 *Nat. Commun.* **7** 12964
[19] You J Q, Hu X, Ashhab S and Nori Franco 2007 *Phys. Rev. B* **75** 140515(R)
[20] Steffen M, Kumar S, DiVincenzo D P, *et al.* 2010 *Phys. Rev. Lett.* **105** 100502
[21] Nguyen L B, Lin Y, Somoroff A, Mencia R, Grabon N and Manucharyan V 2019 *Phys. Rev. X* **9** 041041
[22] Manucharyan V E, Koch J, Glazman L I and Devoret M H 2009 *Science* **326** 113
[23] Martinis J M, Nam S, Aumentado J and Urbina C 2002 *Phys. Rev. Lett.* **89** 117901
[24] Yu Y, Han S, Chu X, Chu S and Wang Z 2002 *Science* **296** 889
[25] Ramos R C, Gubrud M A, Berkley A J, Anderson R J, Lobb J C and Wellstood C F 2001 *IEEE T. Appl. Supercon.* **11** 998
[26] Brito F and Caldeira A O 2008 *New J. Phys.* **10** 115014
[27] Martinis J M, Devoret M H and Clarke J 1985 *Phys. Rev. Lett.* **55** 1543
[28] Martinis J M 2009 *Quantum Inf. Processing* **8** 81
[29] Lang K M, Nam S, Aumentado J, Urbina C and Martinis J M 2003 *IEEE T. Appl. Supercon.* **13** 989
[30] Simmonds R W, Lang K M, Hite D A, Nam S, Pappas D P and Martinis J M 2004 *Phys. Rev. Lett.* **93** 077003
[31] Brooks P, Kitaev A and Preskill J 2013 *Phys. Rev. A* **87** 052306
[32] Gyenis A, Mundada P S, Di Paolo A, Hazard T M, You X, Schuster D I, Koch J, Blais A and Houck A 2021 *Phys. Rev. X* **2** 010339
[33] Pechenezhskiy I V, Mencia R A, Nguyen L B, Lin Y and Manucharyan V E 2020 *Nature* **585** 368
[34] Chang J B, Vissers M R, Córcoles A D, Sandberg M, Gao J, Abraham D W, Chow J M, Gambetta J M, Rothwell M B, Keefe G A, Steffen M and Pappas D P 2013 *Appl. Phys. Lett.* **103** 012602
[35] Takita M, Córcoles A D, Magesan E, *et al.* Abdo B, Brink M, Cross A, Chow J M, and Gambetta J M 2016 *Phys. Rev. Lett.* **117** 210505
[36] Rigetti C, Gambetta J M, Poletto S, Plourde B L T, Chow J M, Córcoles A D, Smolin J A, Merkel S T, Rozen J R, Keefe G A, Rothwell M B, Ketchen M B and Steffen M 2012 *Phys. Rev. B* **86** 100506(R)
[37] Pop I M, Geerlings K, Catelani G, Schoelkopf R, Glazman L and Devoret M H 2014 *Nature* **508** 369
[38] Jin X Y, Kamal A, Sears A P, Gudmundsen T, Hover D, Miloshi J, Slattery R, Yan F, Yoder J, Orlando T P, Gustavsson S and Oliver W D 2015 *Phys. Rev. Lett.* **114** 240501
[39] Dial O, McClure D T, Poletto S, *et al.* 2016 *Supercond. Sci. Tech.* **29** 044001
[40] Tsioutsios I, Serniak K, Diamond S, Sivak V V, Wang Z, Shankar S, Frunzio L, Schoelkopf R J and Devoret M H 2020 *AIP Adv.* **10** 065120
[41] Barends R, Kelly J, Megrant A, *et al.* 2014 *Nature* **508** 500
[42] Dunsworth A, Megrant A, Quintana C, *et al.* 2017 *Appl. Phys. Lett.* **111** 022601
[43] Yan F, Gustavsson S, Kamal A, *et al.* 2016 *Nat. Commun.* **7** 12964
[44] Krantz P, Kjaergaard M, Yan F, Orlando T P, Gustavsson S and Oliver W D 2019 *Appl. Phys. Rev.* **6** 021318
[45] Gu X, Kockum A F, Miranowicz A, Liu Y and Nori F 2017 *Phys. Rep.* **718–719** 1

[46] Blais A, Huang R, Wallraff A, Girvin S M and Schoelkopf R J 2004 *Phys. Rev. A* **69** 062320
[47] Sank D T 2014 *Fast, accurate state measurement in superconducting qubits* (Ph.D. Dissertation) (Santa Barbara: University of California, Santa Barbara)
[48] McKay D C, Wood C J, Sheldon S, Chow J M and Gambetta J M 2017 *Phys. Rev. A* **96** 022330
[49] Sakurai J J and Napolitano J 2011 *Modern Quantum Mechanics*, 2nd edn. (San Francisco: Pearson) p. 177
[50] Nielsen M A and Chuang I L 2010 *Quantum Computation and Quantum Information*, 10th Anniversary edn. (Cambridge: Cambridge University Press) p. 194
[51] Loss D and DiVincenzo D P 1998 *Phys. Rev. A* **57** 120
[52] Schuch N and Siewert J 2003 *Phys. Rev. A* **67** 032301
[53] DiCarlo L, Chow J M, Gambetta J M, Bishop L S, Johnson B R, Schuster D I, Majer J, Blais A, Frunzio L and Girvin S M 2009 *Nature* **460** 240
[54] Kelly J, Barends R, Campbell B, *et al.* 2014 *Phys. Rev. Lett.* **112** 240504
[55] Li S, Castellano A D, Wang S, Wu Y, Gong M, Yan Z, Rong H, Deng H, Zha Chen, Guo C, Sun L, Peng C, Zhu X and Pan J 2019 *npj Quantum Inform.* **5** 84
[56] Barends R, Quintana C M, Petukhov A G, *et al.* 2019 *Phys. Rev. Lett.* **123** 210501
[57] Rigetti C and Devoret M 2010 *Phys. Rev. B* **81** 134507
[58] Chow J M, Córcoles A D, Gambetta J M, Rigetti C, Johnson B R, Smolin J A, Rozen J R, Keefe G A, Rothwell M B, Ketchen M B and Steffen M 2011 *Phys. Rev. Lett.* **107** 080502
[59] Chow J M, Gambetta J M, Córcoles A D, Merkel S T, Smolin J A, Rigetti C, Poletto S, Keefe G A, Rothwell M B, Rozen J R, Ketchen M B and Steffen M 2012 *Phys. Rev. Lett.* **109** 060501
[60] Paik H, Mezzacapo A, Sandberg M, McClure D T, Abdo B, Córcoles A D, Dial O, Bogorin D F, Plourde B L T, Steffen M, Cross A W, Gambetta J M and Chow J M 2016 *Phys. Rev. Lett.* **117** 250502
[61] Reagor M, Osborn C B, Tezak N, *et al.* 2018 *Sci. Adv.* **4** eaao3603
[62] Li S, Castellano A D, Wang S, Wu Y, Gong M, Yan Z, Rong H, Deng H, Zha C, Guo C, Sun L, Peng C, Zhu X and Pan J 2019 *npj Quantum Inform.* **5** 84
[63] Rol M A, Battistel F, Malinowski F K, Bultink C C, Tarasinski B M, Vollmer R, Haider N, Muthusubramanian N, Bruno A, Terhal B M and DiCarlo L 2019 *Phys. Rev. Lett.* **123** 120502
[64] Hong S S, Papageorge A T, Sivarajah P, Crossman G, Dider N, Polloreno A M, Sete E A, Turkowski S W, da Silva M P and Johnson B R 2020 *Phys. Rev. Lett.* **101** 012302
[65] Xu Y, Chu J, Yuan J, Qiu J, Zhou Y, Zhang L, Tan X, Yu Y, Liu S, Li J, Yan F and Yu D 2020 *Phys. Rev. Lett.* **125** 240503
[66] Kjaergaard M, Schwartz M E, Greene A, *et al.* 2020 arXiv: 2001.08838v3 [quant-ph]
[67] Sheldon S, Magesan E, Chow J M and Gambetta J M 2016 *Phys. Rev. A* **93** 060302
[68] Mckay D C, Filipp S, Mezzacapo A, Magesan E, Chow J M and Gambetta J M 2016 *Phys. Rev. Appl.* **6** 064007
[69] Caldwell S A, Didier N, Ryan C A, *et al.* 2018 *Phys. Rev. Appl.* **10** 034050
[70] Mundada P, Zhang G, Hazard T and Houck A 2019 *Phys. Rev. Appl.* **12** 054023
[71] Chou K S, Blumoff J Z, Wang C S, Reinhold P C, Axline C J, Gao Y Y, Frunzio L, Devoret M H, Jiang L and Schoelkopf R J 2018 *Nature* **561** 368
[72] Rosenblum S, Gao Y Y, Reinhold P, Wang C, Axline J, Frunzio L, Girvin S M, Jiang L, Mirrahimi M, Devoret M H and Schoelkopf R J 2018 *Nat. Commun.* **9** 652
[73] Xu K, Ning W, Huang X, Han P, Li H, Yang Z, Zheng D, Fan H and Zheng S 2021 *Optica* **8** 972
[74] van de Wal C H, ter Haar A C J, Wilhelm F K, Schouten R N, Harmans C J P M, Orlando T P, Lloyd S and Mooji J E 2000 *Science* **290** 773
[75] Clerk A A, Girvin S M, Marquardt F and Schoelkopf R J 2008 *Rev. Mod. Phys.* **82** 1155
[76] Caves C M 1982 *Phys. Rev. D* **26** 1817
[77] Mutus J Y, White T C, Barends R, *et al.* 2014 *Appl. Phys. Lett.* **104** 263513
[78] Macklin C, O'Brien K, Hover D, Schwartz M F, Bolkhovsky V, Zhang X, Oliver W D and Siddiqi I 2015 *Science* **350** 307
[79] Deutsch D 1985 *Proc. R. Soc. Lond. A* **400** 97
[80] Deutsch D and Jozsa R 1992 *Proc. R. Soc. Lond. A* **439** 553
[81] Dicarlo L, Chow J M, Gambetta J M, Bishop L S, Johnson B R, Schuster D I, Majer J, Blais A, Frunzio L, Girvin S M and Schoelkopf R J 2009 *Nature* **460** 240
[82] Shor P W 1994 *Proceedings of 35th Annual Symposium on the Foundations of Computer Science*, November 20-22 1994, Los Alamitos, USA, p. 124
[83] Zalka Christof 1998 arXiv: quant-ph/9806084v1
[84] Lucero E, Barends R, Chen Y, Kelly J, Mariantoni M, Megrant A, O'Malley, Sank D, Vainsencher, Wenner J, White T, Yin Y, Cleland A N and Martinis J M 2012 *Nat. Phys.* **8** 719
[85] Harrow A W, Hassidim A and Lloyd S 2009 *Phys. Rev. Lett.* **103** 150502
[86] Chen C, Shiau S, Wu M and Wu Y 2019 *Sci. Rep. UK* **9** 16251
[87] Lee Y, Joo J and Lee S 2019 *Sci. Rep. UK* **9** 4778
[88] Farhi E, Goldstone J and Gutmann S 2014 arXiv: 1411.4028 [quant-ph]
[89] Guerreschi G G and Matsuura A Y 2019 *Sci. Rep.* **9** 6903
[90] Neeley M, Ansmann M, Bialczak R C, Hofheinz M, Katz N, Lucero E, O'Connell A, Wang H, Cleland A N and Martinis J M 2008 *Nat. Phys.* **4** 523
[91] Chow J M, Gambetta J M, Tornberg L, Koch J, Bishop L S, Houck A A, Johnson B R, Frunzio S M, Girvin S M and Schoelkopf R J 2009 *Phys. Rev. Lett.* **102** 090502
[92] Hou Z, Tang J F, Ferrie C, Xiang G Y, Li C F and Guo G C 2020 *Phys. Rev. A* **101** 022317
[93] Mckay D C, Sheldon S, Smolin J A, Chow J M and Gambetta J M 2019 *Phys. Rev. Lett.* **122** 200502
[94] Helsen J, Wallman J J, Flammia S T and Wehner S 2019 *Phys. Rev. A* **100** 032304
[95] Preskill J 1997 arXiv: 9712048 [quant-ph]
[96] Shor P W 1995 *Phys. Rev. A* **52** R2493(R)
[97] Steane A M 1996 *Phys. Rev. A* **54** 4741
[98] Calderbank A R, Rains E M, Shor P W and Sloane N J A 1997 *Phys. Rev. Lett.* **78** 405
[99] Nielsen M A and Chuang I L 2010 *Quantum Computation and Quantum Information*, 10th Anniversary edn. (Cambridge: Cambridge University Press) p. 453
[100] Dennis E, Kitaev A, Landahl A and Preskill J 2002 *J. Math Phys.* **43** 4452
[101] Wang D S, Fowler A G and Hollenberg L C 2011 *Phys. Rev. A* **83** 020302
[102] Fowler A G, Mariantoni M, Martinis J M and Cleland A N 2012 *Phys. Rev. A* **86** 032324
[103] Ghosh J, Fowler A G, Martinis J M and Geller M R 2013 *Phys. Rev. A* **88** 062329
[104] Brown N C, Cross A and Brown K R 2020 *IEEE International Conference on Quantum Computing and Engineering*, October 11–16, 2020, Broomfield, USA 286
[105] Kelly J, Barends R, Fowler A G, *et al.* 2015 *Nature* **519** 66
[106] Takita M, Cross A W, Córcoles A D, Chow J M and Gambetta J M 2017 *Phys. Rev. Lett.* **119** 180501
[107] Andersen C A, Remm A, Lazar S, Krinner S, Lacroix N, Norris G J, Gabureac M, Eichler C and Wallraff A 2020 *Nat. Phys.* **16** 875
[108] Chuang I L, Leung D W and Yamamoto Y 1997 *Phys. Rev. A* **56** 1114
[109] Gottesman D, Kitaev A and Preskill J 2001 *Phys. Rev. A* **64** 012310
[110] Mirrahimi M, Leghtas Z, Albert V V, Touzard S, Schoelkopf R J, Jiang L and Devoret M H 2014 *New J. Phys.* **16** 045014
[111] Wang C, Gao Y Y, Reinhold P, Heeres R W, Ofek N, Chou K, Axline C, Reagor M, Blumoff J, Sliwa K M, Frunzio L, Girvin S M, Jiang L, Mirrahimi M, Devoret M H and Schoelkopf R J 2016 *Science* **352** 1087
[112] Rosenblum S, Gao Y Y, Reinhold P, Wang C, Axline C J, Frunzio L, Girvin S M, Jiang L, Mirrahimi M, Devoret M H and Schoelkopf R J 2018 *Nat. Commun.* **9** 652
[113] Hu L, Ma Y, Cai W, Mu X, Xu Y, Wang W, Wu Y, Wang H, Song Y P, Zou C L, Girvin S M, Duan L M and Sun L 2019 *Nat. Phys.* **15** 503
[114] Ma Y, Xu Y, Mu X, Cai W, Hu L, Wang W, Pan X, Wang H, Song Y P, Zou C L and Sun L 22020 *Nat. Phys.* **16** 827
[115] Feynman R P 1982 *Int. J. Theor. Phys.* **21** 467
[116] Lloyd S 1996 *Science* **273** 1073
[117] Paraoanu G S 2014 *J. Low. Temp. Phys.* **175** 633
[118] Buluta I and Nori F 2009 *Science* **326** 108
[119] Houck A A, Türeci H E and Koch J 2012 *Nat. Phys.* **8** 292

[120] Raftery J J 2017 *Nonequilibrium Quantum Simulation in Circuit QED* (Ph.D. dissertation) (Princeton: Princeton University)
[121] Xu K, Sun Z H, Liu W, Zhang Y R, Li H, Dong H, Ren W, Zhang P, Nori F, Zheng D, Fan H and Wang H 2020 *Sci. Adv.* **6** eaba4935
[122] Liu W W, Zheng D N and Zhao S P 2018 *Chin. Phys. B* **27** 027401
[123] Ward N J, Kassal I and Aspuru-Guzik A 2009 *J. Chem. Phys.* **130** 194105
[124] Kassal I, Whitfield J D, Perdomo-Ortiz A, Yung M H and Aspuru-Guzik A 2011 *Annu. Rev. Phys. Chem.* **62** 185
[125] Brown K L, Munro W J and Kendon V M 2010 *Entropy* **12** 2268
[126] Nielsen M A and Chuang I L 2010 *Quantum Computation and Quantum Information*, 10th Anniversary edn. (Cambridge: Cambridge University Press) p. 206
[127] Suzuki M 1995 *Phys. Lett. A* **201** 425
[128] Babbush R, McClean J, Wecker D, Aspuru-Guzik A and Wiebe N 2015 *Phys. Rev. A* **91** 022311
[129] Clark C R, Metodi T S, Gasster S D and Brown K R 2009 *Phys. Rev. A* **79** 062314
[130] Somma R, Ortiz G, Gubernatis J E, Knill E and Laflamme R 2002 *Phys. Rev. A* **65** 042323
[131] Kjaergaard M, Schwartz M E, Braumüller J, Krantz P, Wang J I J, Gustavsson S and Oliver W D 2020 *Annu. Rev. Conden. Mater. Phys.* **11** 369
[132] Lamata L, Parra-Rodriguez A, Sanz M and Solano E 2018 *Adv. Phys. X* **3** 519
[133] Girvin S M and Yang K 2019 *Modern Condensed Matter Physics* (Cambridge: Cambridge University Press) p. 486
[134] Heras U L, García-Álvarez L, Mezzacapo A, Solano E and Lamata L 2015 *EPJ Quantum Technol.* **2** 8
[135] Barends R, Lamata L, Kelly J, *et al.* 2015 *Nat. Commun.* **6** 7654
[136] Dallaire-Demers P L and Wilhelm F K 2016 *Phys. Rev. A* **94** 062304
[137] Dallaire-Demers P L and Wilhelm F K 2016 *Phys. Rev. A* **93** 032303
[138] Reiner J M, Marthaler M, Braumüller J, Weides M and Schön G 2016 *Phys. Rev. A* **94** 032338
[139] Cai Z 2020 *Phys. Rev. Appl.* **14** 014059
[140] Roushan P, Neil C, Tangpanitanon, *et al.* 2017 *Science* **358** 1175
[141] Ma R, Saxberg B, Owens C, Leung N, Lu Y, Simon J and Schuster D I 2019 *Nature* **566** 51
[142] Paredes B, Widera A, Murg V, Mandel O, Fölling S, Cirac I, Shlyapnikov G V, Hänsch T W and Bloch I 2004 *Nature* **429** 277
[143] Yanay Y, Braumüller J, Gustavsson S, Oliver W D and Tahan C 2020 *npj Quantum Inform.* **6** 58
[144] Ye Y, Ge Z, Wu Y, *et al.* 2019 *Phys. Rev. Lett.* **123** 050502
[145] Li S S, Ge Z Y and Fan H 2020 *Phys. Rev. A* **102** 062409
[146] Roushan P, Neill C, Chen Y, *et al.* 2014 *Nature* **515** 241
[147] Schroer M D, Kolodrubetz M H, Kindel W F, Sandberg M, Gao J, Vissers M R, Pappas D P, Polkovnikov A and Lehnert K W 2014 *Phys. Rev. Lett.* **113** 050402
[148] Tan X, Zhao Y, Liu Q, Xue G, Yu H F, Wang Z D and Yu Y 2017 *npj Quantum Mater.* **2** 60
[149] Tan X, Zhang D W, Liu Q, Xue G, Yu H F, Zhu Y Q, Yan H, Zhu S L and Yu Y 2018 *Phys. Rev. Lett.* **120** 130503
[150] Tan X, Zhao Y X, Liu Q, Xue G, Yu H F, Wang Z D and Yu Y 2019 *Phys. Rev. Lett.* **122** 010501
[151] Cai W, Han J, Mei F, Xu Y, Ma Y, Li X, Wang H, Song Y P, Xue Z Y, Yin Z Q, Jia S and Sun L 2019 *Phys. Rev. Lett.* **123** 080501
[152] Cao J, Yi X X and Wang H F 2020 *Phys. Rev. A* **102** 032619
[153] Magazzù, L, Denisov S and Hänggi P 2018 *Phys. Rev. E* **98** 022111
[154] Magazzù, L, Denisov S and Hänggi P 2017 *Phys. Rev. A* **96** 042103
[155] Leppäkangas J, Braumüller J, Hauck M, Reiner J M, Schwenk I, Zanker S, Fritz L, Ustinov A V, Weides M and Marthaler M 2018 *Phys. Rev. A* **97** 052321
[156] Muñoz C S, Kockum A F, Miranowicz A and Nori F 2020 *Phys. Rev. A* **102** 033716
[157] Kockum A F, Miranowicz A, Liberato S D, Savasta S and Nori F 2019 *Nat. Rev. Phys.* **1** 19
[158] Yoshihara F, Fuse T, Ashhab S, Kakuyanagi K, Saito S and Semba K 2017 *Nat. Phys.* **13** 44
[159] Indrajeet S, Wang H, Hutchings M D, Taketani B G, Wilhelm F K, LaHaye M D and Plourde B L T 2020 *Phys. Rev. Appl.* **14** 064033
[160] Wang H, Zhuravel A P, Indrajeet, Taketani B G, Hutchings M D, Hao Y, Rouxinol F, Wilhelm F K, LaHaye M D, Ustinov A V and Plourde B L T 2019 *Phys. Rev. Appl.* **11** 054062
[161] Ivanov D A, Ivanova T Y, Caballero-Benitez S F and Mekhov I B 2020 *Phys. Rev. Lett.* **124** 010603
[162] Filippis G D, Candia A D, Cangemi L M, Sassetti M, Fazio R and Cataudella V 2020 *Phys. Rev. B* **101** 180408(R)
[163] Lanyon B P, Whitfield J D, Gillett G G, Goggin M E, Almeida M P, Kassal I, Biamonte J D, Mohseni M, Powell B J, Barbieri M, Aspuru-Guzik A and White A G 2010 *Nat. Chem.* **2** 106
[164] Cao Y, Romero J, Olson J P, Degroote M, Johnson P D, Kieferová M, Kivlichan I D, Menke T, Peropadre B, Sawaya N P D, Sim S, Veis L and Aspuru-Guzik A 2019 *Chem. Rev.* **119** 10856
[165] Moll N, Barkoutsos P, Bishop L S, Chow J M, Cross A, Egger D J, Filipp S, Fuhrer A, Gambetta J M, Ganzhorn M, Kandala A, Mezzacapo A, Müller P, Riess W, Salis G, Smolin J, Tavernelli I and Temme 2018 *Quantum Sci. Technol.* **3** 030503
[166] Peruzzo A, McClean J, Shadbolt P, Yung M H, Zhou X Q, Love P J, Aspuru-Guzik A and O'Brien J L 2014 *Nat. Commun.* **5** 4213
[167] O'Malley P J J, Babbush R, Kivlichan I D, *et al.* 2015 *Phys. Rev. X* **6** 031007
[168] Colless J I, Ramasesh V V, Dahlen D, Blok M S, Kimchi-Schwartz M E, McClean J R, Carter J, de Jong W A and Siddiqi I 2018 *Phys. Rev. X* **8** 011021
[169] Kandala A, Mezzacapo A, Temme K, Takita M, Brink M, Chow J M and Gambetta J M 2017 *Nature* **549** 242
[170] Google AI Quantum and Collaborators, Arute F, Arya K, *et al.* 2020 *Science* **369** 1084
[171] Pedernales J S, Di Candia R, Ballester D and Solano E 2013 *New J. Phys.* **15** 055008
[172] Mei F, Stojanović V M, Siddiqi I and Tian L 2013 *Phys. Rev. B* **88** 224502
[173] Guo X Y, Yang C, Zeng Y, Peng Y, Li H K, Deng H, Jin Y R, Chen S, Zheng D and Fan H 2019 *Phys. Rev. Appl.* **11** 044080
[174] Guo Q, Cheng C, Sun Z H, Song Z, Li H, Wang Z, Ren W, Dong H, Zheng D, Zhang Y R, Mondaini R, Fan H and Wang H 2020 *Nat. Phys.* **17** 234
[175] Stella L, Santoro G E and Tosatti E 2005 *Phys. Rev. B* **72** 014303
[176] Hauke P, Katzgraber H G, Lechner W, Nishimori H and Oliver W D 2020 *Rep. Prog. Phys.* **83** 054401
[177] Neven H, Denchev V S, Rose G and Macready W G 2009 arXiv: 0912.0779v1 [quant-ph]
[178] Li R Y, Felice R D, Rohs R and Lidar D A 2018 *npj Quantum Inform.* **4** 14
[179] Hernandez M and Aramon M 2017 *Quantum Inf. Process.* **16** 133
[180] Das S, Wildridge A J, Vaidya S B and Track A J 2019 arXiv: 1903.08879v3 [hep-ex]
[181] Mott A, Job J, Vlimant J R, Lidar D and Spiropulu M 2017 *Nature* **550** 375
[182] Rønnow T F, Wang Z, Job J, Boixo S, Isakov S V, Wecker D, Martinis J M, Lidar D A and Troyer M 2014 *Science* **345** 420
[183] Johnson M W, Amin M H S, Gildert S, *et al.* 2011 *Nature* **473** 194
[184] King A D, Carrasquilla J, Raymond J, *et al.* 2018 *Nature* **560** 456
[185] Harris R, Sato Y, Berkley A J, *et al.* 2018 *Science* **361** 162
[186] Jiang S, Britt K A, McCaskey A J, Humble T S and Kais S 2018 *Sci. Rep.* **8** 17667
[187] Albash T and Lidar D A 2018 *Phys. Rev. X* **8** 031016
[188] Mandrà S, Katzgraber H G and Thomas C 2017 *Quantum Sci. Technol.* **2** 038501
[189] Katzgraber H G 2018 *Quantum Sci. Technol.* **3** 030505
[190] Vedral V, Barenco A and Ekert A 1996 *Phys. Rev. A* **54** 147